Ash chemistry in chemical looping process for biomass valorization: A review

Chemical Engineering Journal 478 (2023) 147429

Contents lists available at ScienceDirect

Chemical Engineering Journal

journal homepage: www.elsevier.com/locate/cej

Review

Ash chemistry in chemical looping process for biomass valorization: A review

Yuru Liu [a,1], Ke Yin [a,1], Jiawei Wu [b,1], Daofeng Mei [c,1], Jukka Konttinen [d], Tero Joronen [d], Zhifeng Hu [b,*], Chao He [d,*]

[a] Department of Environmental Engineering, College of Biology and the Environment, Nanjing Forestry University, 159 Longpan Road, Nanjing 210037 China
[b] Key Laboratory for Biobased Materials and Energy of Ministry of Education, College of Materials and Energy, South China Agricultural University, Guangzhou 510642, China
[c] Division of Energy Technology, Department of Space, Earth and Environment, Chalmers University of Technology, Gothenburg 41296, Sweden
[d] Materials Science and Environmental Engineering, Faculty of Engineering and Natural Sciences, Tampere University, Korkeakoulunkatu 8, 33720 Tampere, Finland

ARTICLE INFO

Keywords:
Ash composition
Oxygen carrier
Interaction
Melting and agglomeration
Metals recovery

ABSTRACT

Chemical looping process (CLP) is a novel carbon capture technology for biomass valorization. Low-cost and robust oxygen carrier (OC) is crucial for industrialization of CLP. However, ash in solid fuels will unavoidably deposit on OC and even react with OC, leading to severe agglomeration and sintering which could not only degrade the full functionality of OC but also make the complete separation of ash and OC challenging. In order to holistically elucidate the ash chemistry in CLP, this review has systematically analyzed the effect of ash compositions in biomass on CLP efficiency, the impact of ash components on physicochemical properties and oxygen transfer capacity of OC, as well as the melting and agglomeration behaviors of ash components. Specifically, both inhibition and enhancement effects of various ash components have been illustrated. Particularly, the influence of alkali and alkaline earth metals in biomass ash on agglomeration of OC has been analyzed in detail. Four mechanisms are summarized to explain the agglomeration and melting process, including coating-induced, melting-induced, ash deposition-melting, the layer joint and bridge joint mechanisms. Ultimately, strategies are proposed to effectively mitigate adverse impacts of ash and recycle useful metals for industry use and re-synthesis of OC. To promote future development of CLP, perspectives are provided to guide the novel design of next generation OC in terms of structural and compositional optimization.

1. Introduction

Chemical looping process (CLP) is a novel carbon capture technology where the oxygen for combustion is supplied by a continuous redox reaction of the oxygen carriers (OCs) between fuel reactor and air reactor, so the technology inherently captures CO_2 with a low energy penalty and low NO_x emissions [1]. OCs, typically composed of various transitional metal oxides, supply oxygen for fuel oxidation (Eq. (1)), and then regenerate themselves in the air (Eq. (2)) to achieve cyclic operation.

$$\text{Fuel} + Me_xO_y \rightarrow CO_2 + H_2O + Me_xO_{y-1} \quad (1)$$

$$\text{Air} + Me_xO_{y-1} \rightarrow Me_xO_y + O_2 depleted air \quad (2)$$

Solid fuels generally used for CLP include coal [2], petroleum coke [3], solid wastes (e.g., biomass [4] and sewage sludge [5]). CLP can be further divided into in-situ gasification chemical looping combustion (CLC) and chemical looping oxygen uncoupling. Previous studies have proven that gasification is a rate-limiting step for CLP reactions [6], and hence, highly reactive solid fuels are vital. Biomass [7] gradually becomes a research hotspot in this regard, which has advantages of lower cost, higher reserves and the net negative CO_2 emissions [8]. To date, CLP targeting biomass management, such as biomass chemical looping gasification (BCLG) and biomass chemical looping reforming, have been developed for sustainable biomass valorization.

In the face of large scale BCLG, low-cost OCs are preferred. However, complete separation of biomass/coal ash and the OC is difficult. Ash deposition on OCs can lead to agglomeration and sintering which could degrade the full functionality of OCs. As a result, partial OCs is disposed

* Corresponding authors.
E-mail addresses: huzf@scau.edu.cn (Z. Hu), chao.he@tuni.fi (C. He).
[1] These authors contributed equally as first authors.

https://doi.org/10.1016/j.cej.2023.147429
Received 7 September 2023; Received in revised form 2 November 2023; Accepted 14 November 2023
Available online 18 November 2023

Nomenclature

3DOM OC	three dimensional ordered macroporous oxygen carrier
AAEMs	alkali and alkaline earth metals
BCLG	biomass chemical looping gasification
CLC	chemical looping combustion
CLG	chemical looping gasification
CLP	chemical looping process
FA	fly ash
FBC	fluidized bed combustor
OC	oxygen carrier
OTC	oxygen transfer capacity
SSA	sewage sludge ash

of along with the ash. The typical composition of biomass and coal ash contains Al_2O_3, SiO_2, Fe_2O_3, CaO, MgO, K_2O, Na_2O, TiO_2, etc., as shown in Table 1. Biomass ash contains alkali and alkaline earth metals (AAEMs) which are more prone to cause corrosion, agglomeration anomalies and OC deactivation [9]. The deposition of ash on OCs is not entirely detrimental, because some ash contents, such as Fe_2O_3, $CaSO_4$, can somewhat improve the reactivity of OCs. The severity of reduced active sites of OCs depends on operating temperature, fluidization velocity, particle size, etc. [10].

Ash is a complex solid matrix and varies in components and characteristics depending on the origin and nature of feedstocks. Fig. 1 demonstrates interactions of various ash elements with OC. The presence of ash could either have inhibition effect resulting from ash melting/agglomeration or enhancement effect ascribing to its role as catalyst or perovskites, closely depending on the composition. So far, research on interactions between ash contents and OCs is relatively scattered among individual studies, with a shortage of systematical summary and comparative analysis of findings and data integration. To fill this knowledge gap, the physicochemical interactions between OCs and ash shall be well understood via analyzing the system performance, such as the oxygen transfer capacity (OTC) and mechanical properties of OCs, gas yield, and carbon conversion efficiency, etc. A holistic review on the ash chemistry is incredibly beneficial to minimize negative impacts caused by ashes through necessary process control, and concomitantly explore potential synergies between specific OCs and certain ash components to achieve sustainable application of CLP at large scale.

2. Effect of ash composition on process efficiency

At present, a large part of the database about the effect of ash on OCs is based on the interaction of coal ash with OCs. However, with the increasing potential of global warming, more research has been focused on the use of biomass-based solid waste through CLC or CLG processes. These studies accumulate useful knowledge to expand know-how of interactions between various ashes and OCs.

Table 1
Typical ash compositions in biomass and coal [11–14].

Ash components	Biomass (wt.%)	Coal (wt.%)
SiO_2	22–36	10–54
Al_2O_3	5–15	24–58
Fe_2O_3	3–9	6–12
CaO	9–43	3.9–17
TiO_2	0.3–1.2	0.5–1.9
K_2O	10–25	1.6–3.8
MgO	6–14	0.5–6
Na_2O	0.4–3	0.1–0.8
P_2O_5	3–7	0.1–0.5

The interaction between different ashes and OCs may cause controversial effects [15]. For instance, Azis et al. [16] concluded that adding coal gasification ash to ilmenite reduced the reactivity of OCs, whereas the addition of lignite combustion ash has significantly increased the ilmenite reactivity. The ash components attached to the particle surface can affect the reduction rate of OC, as gas diffusion is impeded by a layer of ash shell. Thus, lower gas conversion was obtained when the OC reactivity is lowered. On the other hand, the attached ash components may catalyze certain reactions or even function as OCs. Besides, ash components may react with OCs to form new compounds that can increase or decrease OTC. Notably, the gas environment in the CLC fuel reactor is different from that in a normal combustion chamber due to limited free oxygen, therefore, the reduction potential is higher. This may result in different ash conversion processes as compared to the normal combustion. In this regard, when examining the interaction between OCs and ashes, a reduction environment with gasification products (e.g., CO and H_2) is preferred. Besides, many studies indicate that coal fly ash (FA) has limited impact on OCs [17].

2.1. Inhibition effect

Ash content and composition vary greatly according to the fuel oxidation used in the process of chemical looping combustion of biomass. The ash contains inorganic matter that remains after the fuel is combusted. The most common elements in biomass ash are calcium, potassium, silicon, magnesium, aluminium, sulphur, iron, phosphorous, chlorine, sodium and trace elements [18]. During biomass combustion, silicon may react with calcium to form calcium silicate that adheres to the surface of the bedding to form a coating. Depending on the composition and physical state of the ash, scaling, slagging and corrosion related problems may occur. Potassium is the main alkali source in biomass ash, which will cause more problems in the biomass reaction process. In biomass fuels with high chlorine content, potassium is easy to react with chlorine to form gaseous potassium chloride. Such substances are often the cause of corrosion and structure in boiler channels. When potassium reacts with a fluidized bed, viscous ash compounds form on the surface of the particles. This causes particles to clump together into larger clumps.

In addition to caking, ash in biomass fuels is more likely to significantly inhibit gas production, oxygen conversion efficiency and fuel combustion efficiency, which is attributed to ash inactivation of OC. Ash components attached to the particle surface may affect oxidation and reduction rates of OC. Ash adhering to OC surface may diffuse and penetrate into particles, resulting in volume expansion and cracking of OC particles, hindering gas diffusion, and thus reducing reaction rate [19]. On the other hand, the reaction of the attached ash component with the OC to form new compounds may reduce the OTC. The formation of iron silicates during the cycle of $CuFe_2O_4$ ferrioxite carriers using hydrogen as fuel reduced the OTC of $CuFe_2O_4$ [20]. Effect of different ash contents on CLC has also been examined in fluidized bed reactor [16]. In the presence of 23 % of the ash load, SiO_2, an inert/inactivated substance in the ash, hindered the gas–solid reaction of ilmenite. When Cu-based OC was mixed with coal ash, solid conversion during oxygen decoupling was reduced [21].

2.2. Enhancement effect

During the CLG process, the presence of ash has also demonstrated some beneficial effects. Different ash components may catalyze or form specific structures that can enhance the performance of OCs and chemical reactions. Some ash species, such as Fe_2O_3, $CaSO_4$, can act as OCs. Bao et al. [22] operated the CLC process using coal ash and iron ore with CO in a fluidized bed reactor. Si-containing species reacted with Fe to form Fe_2SiO_4 and retarded their reactivity. However, Ca-containing ash increased the reactivity because sintering and agglomeration were negligible. Dan et al. [23] showed that CuO can easily react with ash

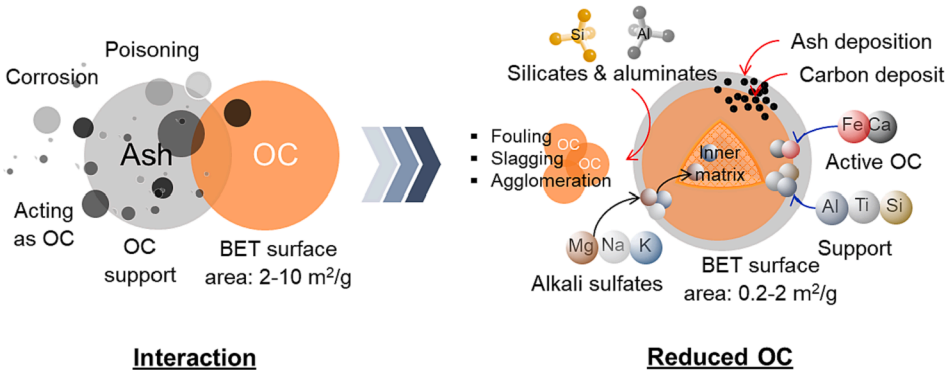

Fig. 1. Potential interactions of ash elements with OC.

species (i.e., Fe_2O_3 and Al_2O_3) to form $CuAl_2O_4$ and $CuFe_2O_4$. The presence of Ca restricted formation of Cu-Al and Cu-Si complex. Similarly, the presence of CaO in coal ash inhibited the reaction of CuO and Al_2O_3 by forming $CaAl_2SiO_8$ [24], thus alleviating the deactivation of CuO. Furthermore, CaO was used as a catalyst for tar cracking [25]. However, CaO has limited lifespan due to its low melting point and issues associated with sintering and carbon deposition [8]. Xu et al. [26] performed CLG using pine sawdust as fuel and sewage sludge ash (SSA) as OC. SSA promoted the fuel conversion owing to the presence of Fe_2O_3 in SSA. The interaction was tested for five consecutive cycles using a "pine sawdust to SSA" ratio of 1:1 at 700 °C. The carbon conversion efficiency and syngas yield in the fifth cycle was found to be higher than that in the first cycle. In addition to the presence of Ca in ash, the presence of transition metals in bottom ash had several advantages of acting as OC and providing high thermal stability [27]. The magnetic fraction was separated from ash constituents and evaluated. The reduction rate and OTC of the extracted magnetic constituent was similar to those of synthetic Fe_2O_3, suggesting that incineration bottom ash could serve as a cost-effective OC for CLP.

Table 2 summarizes the effect of ash on the reactivity of OCs in CLP. Most components of ash have negative effects on CLP, while only a few components of ash can effectively promote CLP reactions, such as Ca- and Fe-containing compounds. Previous studies have shown that the presence of Ca in ash can improve the efficiency of water–air conversion, and calcium sulfate itself can act as OC. Meanwhile, the presence of Ca can limit the formation of other compounds and effectively mitigate deactivation of iron and copper-based OCs. In CLC process, Fe_2O_3 in ash plays a pivotal role in promoting the oxidation–reduction reaction of OC, because it could function as an active OC with a higher oxygen carrying capacity than pure OC.

Table 2
Effect of ash on the reactivity of OCs in CLP.

Feedstock	Key ingredients in ash	OC	Operating parameters	Performance	References
Sewage sludge	K_2O, CaO	Iron ore	Fluidized bed reactor, T: 900 °C	• Gasification rate is maximum in the 14th cycle • OC reactivity increased due to the presence of K in ash • Formation of $KFe_{11}O_{17}$ occurred in 20th cycle • Sintering and spheroidization occurred beyond 25th cycle	[28]
Rape stalk	K_2O, CaO in RSA	Iron ore with 5–40 % rape stalk ash (RSA)	Fluidized bed reactor, T: 900 °C	• Iron ore with 20 % RSA demonstrated best fluidization characteristics • K in ash weakens the Fe-O bond, which results in release of lattice oxygen from OC	[29]
Biomass ash component	Ca, K,Si	Hemtatite (Fe_2O_3), hausmannite (Mn_3O_4), ilmenite (Fe_2TiO_5)	Fixed bed tubular reactor, T: 900 °C	• K_2CO_3 and SiO_2 formed complexes and caused agglomeration • Interaction of ilmenite with ash was found to be minimum	[9]
Syngas	Fe_2O_3, $CaSO_4$	Incinerated bottom ash	Fixed bed tubular reactor, T: 850 °C	• Showed satisfactory stability till 10 cycles; demonstration strong durability of ash • 95 % combustion efficiency was achieved • Fresh and reduced OC revealed similar XRD patterns	[27]
Anthracite coal	$CaSO_4$, Al_2O_3, SiO_2, Fe_2O_3,	CuO@TiO_2-Al_2O_3	Fluidized bed reactor, T: 900 °C	• Presence of CaO in ash prevented the formation of $CuSO_4$ • Agglomeration occurred due to $CaAl_2SiO_7$	[30]
Bituminous Colombian coal	$FeTiO_3$, Fe_3O_4, TiO_2	Ilmenite	Fluidized bed reactor, T: 820–950 °C	• At higher temperatures, gasification and combustion reactions are faster and promoted • The oxygen demand of gases from 5 % to 15 %	[31]
Anthracite, low volatile bituminous, medium volatile bituminous and lignite	CuO	Spray-dried, 60 % CuO	Interconnected fluidized reactors T: 860–950 °C	• Coal is completely burned into CO_2 and H_2O • The carbon capture efficiency increased with fuel reactor temperature	[32]

3. Interaction between OC and ash components

3.1. Physical and chemical characteristics of OC

OC support is another indispensable constituent in CLC. The main function of this support is to provide mechanical strength to enhance its redox stability and agglomeration resistance of OC. OC support material is usually inert with porous structure to allow the diffusion of reactant gases [33]. Synthetic inert materials, such as SiO_2, Al_2O_3, TiO_2, MgO, ZrO_2, have been used as support for multiple cycles. Al_2O_3 is generally preferred over others due to its high mechanical strength and melting point [34]. FA is characterized with high contents of Al_2O_3, SiO_2, MgO and TiO_2. Thus, coal FA was tested as a cost-effective support to OCs. Furthermore, Fe_2O_3 in FA could act as an active OC, while Na and K were promoters for OC [35]. Na in NaCl or Na_2CO_3 also has an ability to reduce SO_2 and NO emissions, thereby improving the sulfur fixation in the fuel reactor [36]. Table 3 compares main physical and chemical characteristics of pure OCs and OCs after interaction with ash components. Aishya et al. [37] first tested the potential of FA as support with 50 % metal loading of CuO, Fe_2O_3 and NiO at 800 °C. It was observed that FA enhanced the thermal stability of OC, while unsupported CuO-based OC was easily agglomerated during the reduction process. Similar enhanced thermal stability was also presented by Skulimowska et al. [38] for a supported CuO-based OC during 42 consecutive cycles without sintering issue. FA is found to be superior to Al_2O_3 due to its role in hindering carbon deposition [33], thereby enhancing the durability of OC. CH_4 conversion of 94–100 % was achieved with minor deactivation after 10 cycles at 800–850 °C. Thus, FA is proved to be an environmentally friendly and cost-effective support to OC during long term operation. The melting temperature of ash components is in the following order: $Al_2O_3 > MgO > CaO > P_2O_5 > Na_2O > K_2O$. Thus, the presence of Al, Mg, Ca might elevate the melting point while P, Na and K can lead to sintering and agglomeration [11] due to their lower melting point. This issue can be solved either by separating the problematic ash components via adsorption processes or by adding inert species to elevate its melting point. To inhibit the sintering of OCs with the ash species, some OCs was fabricated into the form of ferrites and perovskites which favored the resistance against sintering. CaO has excellent catalytic reactivity, however, when being used alone, it cannot sustain operating temperature above 900 °C [39]. However, this issue can be mitigated by mixing with iron and forming calcium ferrites (i.e., $CaFe_2O_4$, $Ca_2Fe_2O_5$) [40]. Furthermore, calcium ferrites could facilitate H_2 generation and reduce the tar formation [41]. Besides, MgO enhanced the oxygen release capacity of ferrites [42]. Cu-based metal oxides usually suffer from sintering and de-fluidization issues as a result of lower melting point. However, combining it with Fe_2O_3 will enhance its mechanical stability [43]. Bimetallic oxides with special structure (spinel and perovskites) can enhance the reactivity and thermal stability, thus shattering the boundedness of single metal oxide. Siriwardane et al. [44] investigated that $CaFe_2O_4$ and $BaFe_2O_4$ exhibited higher reactivity and selectivity with coal than syngas, thus making them suitable for CLG. Thus, bimetallic components resulting from the interaction of ash components with active OC may be beneficial due to the synergy. The reaction between OC and ash can not only enhance the physical and chemical characteristics of OC, but also cause detrimental effect to OC. The addition of SiO_2-rich wheat straw ash led to a decreased reactivity of OC and caused serious particle sintering of OC [32]. SiO_2, CaO and K_2O in FA can inhibit the formation of low melting point of OC, and even cause the sintering and agglomeration of OC [45].

Table 3
Comparison of physical and chemical characteristics of pure OC and OC after interaction with ash components.

Pure OCs and main characteristics		OC after interaction with ash components	References
CuO	• Easily agglomerated	• Enhanced thermal stability	[37]
Al_2O_3	• Carbon deposition	• Enhanced thermal stability • No sintering • Enhanced durability of OC • Improved CH_4 conversion rate	[38]
Fe_2O_3	• Poor sulfur fixation in the fuel reactor	• Reduced SO_2 and NO emissions • Improved sulfur fixation	[36]
CaO	• Low operating temperature	• High resistance against sintering • Enhanced oxygen release capacity • Facilitated H_2 generation • Reduced tar formation	[40]
Cu-based OC	• Lower melting point • Sintering and desulfurization	• Enhanced reactivity and thermal stability • Enhanced mechanical stability	[43]
Iron ore	• High fuel conversion efficiency	• SiO_2-rich ash led to potassium silicates • Lower SiO_2 ash promoted fuel conversion	[32]
Fe_4Al_6	• Sufficient oxygen-carrying capacity • High reactivity and durability	• Inhibition effect by forming low-melting-point compounds • Enhancement effect through formation of specific structure • Neutral effect by integrating with OC	[45]
Fe_2O_3 and Fe_3O_4	• Better reaction activity	• A "bridge" formation and increased agglomeration • Agglomeration and deactivation	[46]

Eqs. (3) – (11) describe the interaction of Fe-based OCs with various ash components to form low melting point complex components. Formation of these compounds are detrimental since they can agglomerate and retard the reaction rate in the CLC process. Since Eqs. (10) and (11) usually occur at 1200–1300 °C [47], formation of such complexes is negligible during the CLC process which is normally operated at temperature lower than 1000 °C. Moreover, intra-interaction of ash components makes this issue more complicated. In the heat transfer process, KCl, K_2SO_4 and Na_2SO_4 were detrimental since they started to melt at low temperature around 823–944 K [48–50], resulting in strong ash deposition. The mechanism of ash agglomeration into two sections: (a) coating-induced agglomeration and (b) melting-induced agglomeration [10]. The former occurred when ash species interact with bed materials, while the latter took place when silicon and alkali metals in ash produce eutectic melt.

$$Fe_2O_3 + MgO \rightarrow MgFe_2O_4 \quad (3)$$

$$Fe_2O_3 + K_2O \rightarrow K_2Fe_{22}O_{34}/K_2Fe_{10}O_{16}/K_2Fe_4O_7 \quad (4)$$

$$Fe_2O_3 + K_2O + Al_2O_3 + SiO_2 \rightarrow KAlSi_3O_8 \quad (5)$$

$$Fe_2O_3 + CaO \rightarrow CaFe_2O_4 \quad (6)$$

$$Fe_2O_3 + CaO + Al_2O_3 \rightarrow CaFeAl_2O_5/CaAl_2Fe_4O_{10} \quad (7)$$

$$Fe_2O_3 + Al_2O_3 \rightarrow FeAl_2O_4/Fe_4Al_6 \quad (8)$$

$$Fe_2O_3 + Al_2O_3 + SiO_2 \rightarrow FeAl_2O_4/Fe_4Al_6/FeAl_2SiO_6 \quad (9)$$

$$Fe_2O_3 + SiO_2 \rightarrow Fe_2Si_2O_4 \quad (10)$$

$$Fe_2O_3 + Al_2O_3 + SiO_2 + CaO \rightarrow CaAl_2Fe_4O_{10}/CaAl_8Fe_4O_{19}/Ca_2Al_2SiO_7 \quad (11)$$

3.2. Oxygen transfer capacity

Based on the amount and distribution of active metal sites presented

in OC, OC structure and their origin, OCs are classified into different groups, including mono-metal oxides, mixed metal oxides, natural ores, minerals and scrap oxides [51]. Understanding interactions between OCs and ashes is essential to prevent coagulation and backflow.

Table 4 summaries the empirical OTC of different OCs in previous studies. Fe-based OCs have weak redox properties and low methane conversion, but Fe-based OCs are considered viable for CLC applications because they are inexpensive and environmentally benign. Subsequently, the Fe-based OC showed two important properties, namely, high resistance to agglomeration and low tendency of carbon deposition. Thus, OC activity can be controlled and maintained. Fe-based OCs exhibit different oxidation states, such as Fe_2O_3, Fe_3O_4 and FeO. It is important to note that the conversion of Fe_2O_3 and Fe_3O_4 is only suitable for the oxidation of methane in interconnected fluidized bed reactors, which further promotes the production of syngas to avoid being reduced to FeO or metallic Fe. The OTC of Fe-based OC in CLC of coal can reach 86 % of the theoretical value [52]. Due to good fluidization, Fe-based OC may not form agglomeration in the circulation process.

In general, Cu-based OC has good reactivity and low temperature combustion characteristics. It has been reported that the OTC of Cu-based oxides may be lowered when they are in the form of a spinel-type structure. For example, a ratio of Al_2O_3 to CaO at 0.82 in OC resulted in an OTC of about 2.0 wt%, which was approximately their theoretical value, however, the OTC declined along an increasing redox cycles as the ratio was gradually increased to 9.44 [53]. On the other hand, due to the use of less Al, $CuAl_2O_4$ can be formed, so the OTC will be reduced as well. However, with the presence of calcium, the interaction between Cu and Al can be well avoided. Despite limited study on the interaction of Ni-based OC with ash, recent research implied that ash did not have significant effect on the reactivity of Ni-based OC [61].

4. Melting and agglomeration behaviors

Although some biomass ashes can catalyze and improve the CLG performance to a certain extent, the melting and agglomeration of OCs caused by biomass ash can seriously hinder the long-term stable operation of CLG. Open literature has shown that some ash elements are transformed into low melting point substances at high temperature, and then adhere to other particles or react with other substances to form agglomerates.

4.1. Aaems

AAEMs usually represent K, Ca, Na and Mg in biomass because the amount of K, Na, Ca and Mg accounts for the vast majority of AAEMs. AAEMs are the most abundant trace elements in biomass ash which often have a certain catalytic effect in CLG [63]. Ca and Mg in biomass could effectively improve the gasification efficiency and reduce the reaction activation energy during CLG [64,65], while AAEMs could promote the gasification reaction of pyrolysis coke [66].

However, AAEMs also have adverse effects on the reaction process. Under the action of Cl and S, AAEMs compounds usually exist in gaseous form in flue gas at high temperature [67], which is easy to condense on the heating surface and adhere to the FA to form slagging [68]. AAEMs in biomass is easy to react with Si to form eutectic compounds with low melting point, leading to the agglomeration of OC [69]. High contents of Fe_2O_3, CaO and MgO would reduce the ash melting point and sintering activation energy of ash particles, improving the sintering rate of ash particles [70]. AAEMs in biomass remained in the solid residue in the form of alkali metal oxide at high temperature, resulting in coking and slagging during reaction [71]. Meanwhile, a high content CaO would form a film to cover the OC and the film can protect the OC from agglomeration to some extent.

During BCLG, AAEMs in ash will react with OC or bed material to form alkali metal silicate with a low melting point. At high temperature, the molten silicate is easy to aggregate and adhere to other particles to form larger agglomerates. Stanislav et al. [72] analyzed the initial deformation temperature (DT) and hemispherical temperature (HT) of 55 kinds of biomass ashes in the biomass ash chemical classification system. As shown in Figs. 2 and 3, DT and HT are high when the main components in biomass ash are CaO and MgO. On the contrary, DT and HT are low when the main components are Na_2O and K_2O. This is because Ca and Mg usually react with SiO_2 in BCLG to produce silicate compounds with a high melting point. However, the K and Na tends to react with SiO_2 and S to generate silicate compounds and sulfate compounds with a low melting point. These low melting point compounds tend to adhere to the surface of ash particles, increasing the adhesion of ash particles and forming agglomerations. However, most of Na (K) will be directly sublimated into gaseous Na (K) or released into the gas phase in the form of NaCl (KCl) during CLG [73], whereas only a few will be converted into silicate at high temperature. Moreover, Na in the gas phase has an obvious tendency to deposit, resulting in the agglomeration

Table 4
Oxygen transfer capacity (OTC) of the solid residues retrieved from fuel reactor and air reactor.

Components	Method	OC-Ash	OTC (wt. %)	References
Fe_2O_3/Fe_3O_4	Spray drying	Fe_2O_3	6.94	[54]
Fe_2O_3/FeO	Spray drying	Fe_2O_3	11.33	[55]
Fe_2O_3/ $MgFe_2O_4$	Impregnation	Fe_2O_3-Mg	0.1166	[56]
$Fe_2O_3/CaFe_2O_4$	Electric melting	Fe_2O_3-Ca	0.222	[57]
Fe_2O_3/Al_2O_3	Spray drying	Fe_2O_3-Al	7.51	[54]
$Fe_2O_3/FeAl_2O_4$	Impregnation	Fe_2O_3- Al	0.1169	[56]
$Fe_2O_3/FeAl_6$	Impregnation	Fe_2O_3- Al	3.3	[58]
$Fe_2O_3/Fe_2Si_2O_4$	Co-precipitation and coating	Fe_2O_3- Si	3.5	[59]
CaO/ $Ca_2Al_2SiO_7$	Combustion synthesis	CaO-Al	0.76	[60]
CuO/Cu_2O	Conventional sol–gel	CuO/Cu_2O	16.7	[61]
NiO/Ni	Spray drying	NiO	5.0	[62]

The "OC-Ash" denotes the OC and ash couple, e.g., Fe_2O_3-Mg being composed of Fe_2O_3 and MgO.

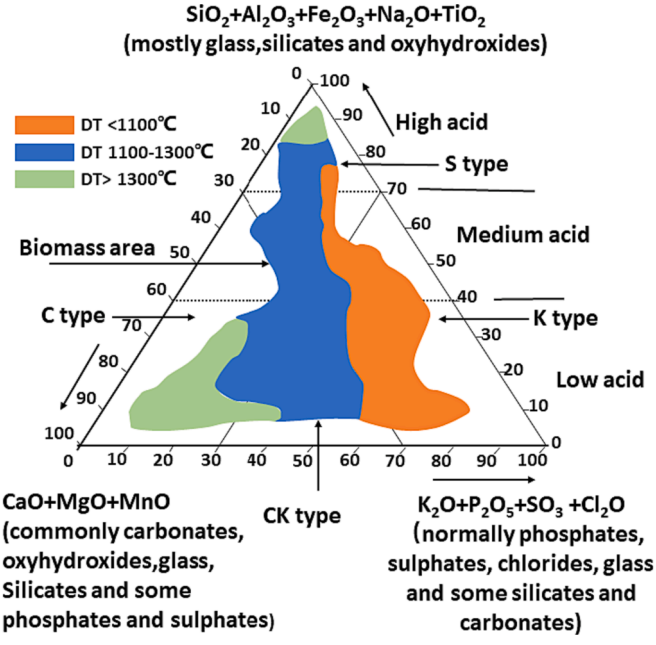

Fig. 2. Areas of low (<1100 °C), medium (1100–1300 °C) and high (>1300 °C) initial deformation ash fusion temperatures for 55 varieties of biomass in the chemical classification system of biomass ash (wt.%) [14].

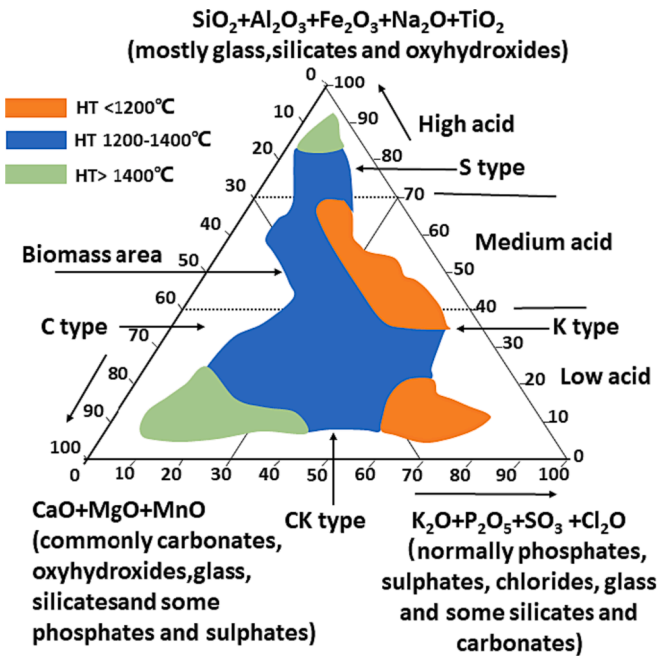

Fig. 3. Areas of low (<1200 °C), medium (1200–1400 °C) and high (>1400 °C) hemispherical ash fusion temperatures for 60 varieties of biomass in the chemical classification system of biomass ash (wt.%) [14].

of ash particles.

As shown in Tables 5 and 6, with the increase of CaO content in biomass, the DT and HT of biomass are higher, indicating that the presence of Ca increases the melting point of biomass ash because of the formation of calcium silicate with a high melting point. Meanwhile, CaO will form a thin film under certain circumstances to cover the OC and inhibit agglomeration. With the increase of K_2O and Na_2O contents in biomass, the DT and HT of biomass are lower, indicating that the presence of K and Na reduces the melting point of biomass ash as a result of the formation of K and Na silicates with a lower melting point. In addition, the MgO content has little effect on DT and HT of the biomass ash.

Alkali silicate with low melting point is the main factor of agglomeration in OC. Moreover, under the influence of AAEMs, the growth and combination of OC grains is also one of the factors affecting agglomeration. Because of the influence of Ca and Mg, the crystal size of OC particles increased gradually and then formed agglomeration to some extent [79]. The outward development of calcium sulfate crystal in the pores and on particle surface accelerated the blockage of pores [80], making the product crystal structure more compact and thus forming larger agglomerates.

Interaction between alkali metals and alkaline earth metals is also one of the factors affecting agglomeration. Sand particles were completely embedded in the internal agglomerate, while the sand particles were connected through limited contacting points in the outer part of the agglomerate [81]. Agglomerates were often shown as hollow structures. The interior of agglomerates was rich in K and Na, which showed an obvious melting phenomenon because of K and Na compounds which have a low melting point. On the contrary, Ca and Mg were concentrated outside the agglomerate, which showed non-molten or partially molten ash structure due to Ca- and Mg-bearing compounds with high melting point [82]. Consequently, the K- and Na-bearing compounds in ash firstly adhere to the surface of OC and gradually form a molten inner layer, while Ca and Mg are introduced to the surface of OC and form $CaAl_2Si_2O_8$ and $Mg_4Al_{10}Si_2O_{23}$ with lower melting point with OC, forming the molten outer layer.

4.2. Other elements

Chlorine (Cl) is the most important non-alkali element in the process of biomass utilization, which can cause serious corrosions to the heat-exchangers surface. In addition, Cl promotes the migration of many inorganic substances, especially K and Na [74]. In most cases, Cl promotes the transport of AAEMs from the interior of biomass to the surface to form sulfate or silicate. At the same time, the presence of Cl also promotes the volatilization of AAEMs in gaseous form and the formation of adsorption particles. Therefore, controlling the Cl content in biomass ash is helpful to reduce the agglomeration caused by AAEMs.

Si and S are essential elements for the conversion of AAEMs to low melting point silicates and sulfates. Hu et al. [83] found that Na, K, Ca, Mg, S and Si were enriched in the low temperature zone of the boiler, and their enrichment helped form sulfates which resulted in the agglomeration of ash particles. Low melting point compounds, e.g., K_2SO_4, NaCl and KCl, will deposit on the heat-exchange surface or adhere to the surface of ash particles, increasing the adhesion of ash particles.

The presence of S will lead to the vulcanization of the OC, resulting in the reduction of the specific surface area and pore volume. At the same time, vulcanization will smooth the surface of OC and reduce the porosity. Iron ore had vulcanization reaction and produced FeS during the chemical looping reaction of sulfur-containing gas with iron ore as OC [84]. Ni_3S_2 with a low melting point was produced during the reaction between H_2S and NiO [85], which led to liquid-phase sintering on the surface of OC and the deactivation of OC.

Table 5
Ash fusion temperatures (FT, °C) and chemical ash composition (wt.%) from 105 varieties of biomass arranged into three initial deformation temperature ranges [72,74–78].

DT range	DT	HT	FT	SiO_2	CaO	K_2O	MgO	SO_3	Na_2O
<1100									
Mean	916	1189	1247	33.01	13.04	30.00	5.98	4.28	2.14
Minimum	700	975	1025	1.65	2.46	9.49	1.67	0.41	0.14
Maximum	1074	1395	1400	77.20	44.32	63.90	14.10	25.74	19.88
1100–1300									
Mean	1200	1287	1306	27.67	31.34	13.78	5.40	3.06	2.46
Minimum	1100	1195	1210	4.48	2.41	0.23	1.10	0.01	0.12
Maximum	1277	1519	1527	68.18	83.46	42.79	13.80	9.70	15.77
>1300									
Mean	1421	1514	1527	23.81	47.89	8.33	5.89	2.04	1.50
Minimum	1309	1380	1395	1.86	0.97	0.16	0.19	0.74	0.09
Maximum	1565	1605	1620	94.48	77.31	23.40	14.57	3.77	4.84

Mean, minimum and maximum represent the mean, minimum and maximum temperature in each temperature range, respectively.

Table 6
Ash fusion temperatures (FT, °C) and chemical ash composition (wt.%) for 60 varieties of biomass arranged into three hemispherical temperature ranges [72,74–78].

HT range	DT	HT	FT	SiO_2	CaO	K_2O	MgO	SO_3	Na_2O
<1200									
Mean	966	1101	1161	41.88	11.45	25.25	4.52	2.90	1.07
Minimum	700	975	1000	7.87	2.98	0.23	1.67	0.83	0.16
Maximum	1180	1195	1280	66.25	26.81	53.38	14.10	5.17	3.52
1200–1400									
Mean	1113	1284	1306	25.69	26.41	20.58	6.09	3.83	2.83
Minimum	775	1205	1208	0.02	2.41	3.16	1.10	0.01	0.12
Maximum	1320	1395	1400	77.20	57.74	63.90	13.80	25.74	19.88
>1400									
Mean	1392	1520	1531	23.29	48.02	7.89	5.51	2.07	1.49
Minimum	1100	1440	1472	1.86	0.97	0.16	0.19	0.74	0.09
Maximum	1565	1605	1620	94.48	83.46	23.40	14.57	3.77	4.84

In summary, most of these elements discussed are detrimental to OCs, such as easily causing agglomeration. Besides, corrosion resulting from sulfur and chlorine must be carefully considered when high sulfur and chlorine fuels are used in CLP.

4.3. Mechanism of melting and agglomeration process

At present, there are generally four mechanisms or methods to explain the agglomeration and melting process: (1) coating-induced, (2) melting-induced, (3) ash deposition-melting mechanism, (4) layer joint and bridge joint mechanisms.

4.3.1. Coating- and melting-induced agglomeration

Fig. 4 shows agglomeration in CLG based on the coating-induced and melt-induced mechanisms. The coating-induced agglomeration is described as follows: the ash produced by biomass combustion is deposited on the bed particles, and then reacts with the small particles attached to the bed material, the condensed alkali metal molecules and gaseous alkali metal molecules to form a coating [10]. The melting-induced agglomeration is induced by the collision between larger molten ash particles and bed particles. Despite some difference, the two mechanisms are not contradictive. Under normal conditions, the active metal components are evenly dispersed on OC. At high temperature, alkali silicate with low melting point formed from the reaction of alkali metals (e.g., K and Na) with OC will cover OC and lead to agglomeration [81]. Billen et al. [86] reported that agglomeration during the combustion of phosphorus enriched poultry litter in a fluidized bed combustor (FBC). Both coating and melting induced agglomeration occurred. P_2O_5 and CaO formed a thermodynamically stable $Ca_3(PO_4)_2$ in the ash. This reduced the amount of calcium silicates in the ash and resulted in K/Ca silicate mixtures exhibiting a lower melting point. On the other hand, in-bed agglomeration is caused by the presence of unstable low melting HPO_4^{2-} and $H_2PO_4^-$ salts present in the fuel. In the hot FBC, these salts may melt, possibly causing bed particles to stick together, which may subsequently react with calcium salts in bed ash to form stable $Ca_3(PO_4)_2$ solid bridges between multiple particles. Meanwhile, the ash in the molten state will adhere to the OC and form large aggregates, making the OC inactive [63]. According to Section 4.1, it can

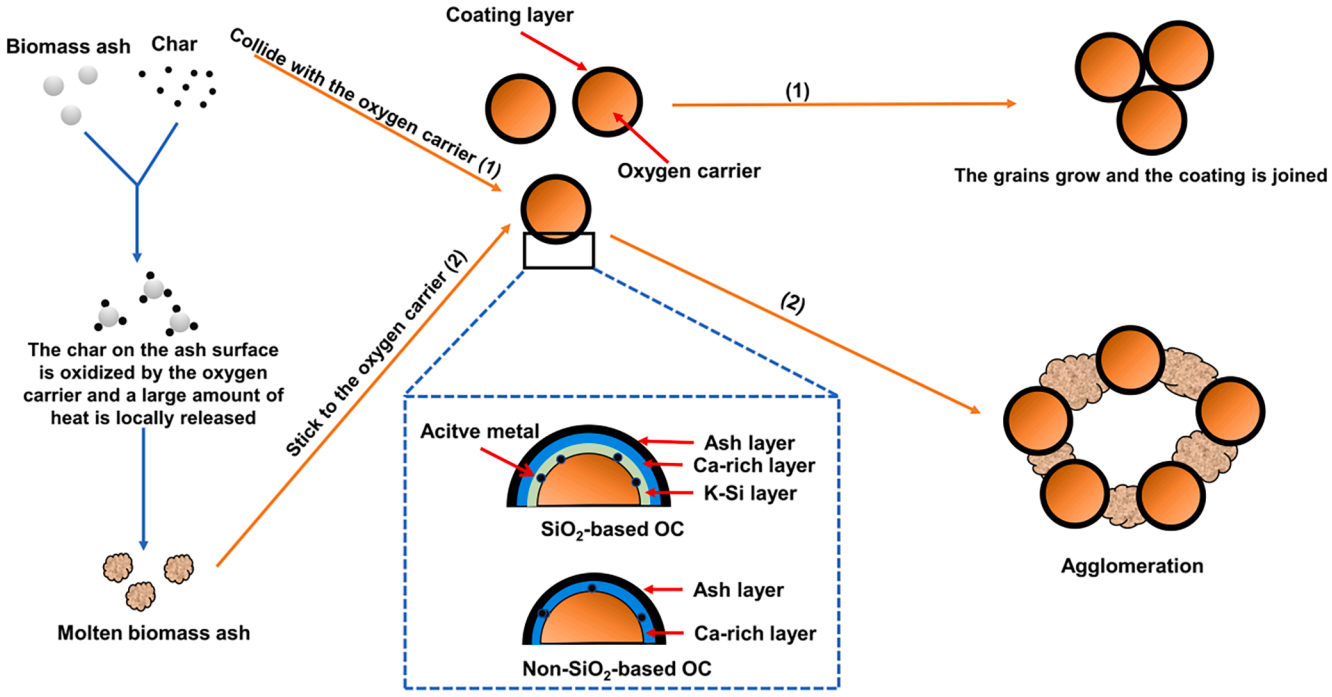

Fig. 4. Agglomeration in CLG based on the coating-induced and melt-induced mechanisms [10]: (1) biomass ash colliding with OC and (2) molten biomass ash sticking to OC.

be deduced that the melting-induced inactivation occurs earlier and will be more fatal than the coating-induced inactivation in CLG.

4.3.2. Ash deposition-melting mechanism

Biomass ash is deposited on the surface of bed particles during the combustion process, and then gradually embeds into molten particles to form agglomerates [87]. At present, there are two opposite versions of this mechanism. On the one hand, the alkali-rich elements released from biomass, especially K, are easy to form fine particles or vapor. They collide and react with silicon and silicates, forming alkali silicate and alkali aluminosilicate, which can increase the viscosity of biomass particles. On the other hand, in biomass combustion, the alkaline chloride released from biomass is transformed into alkaline sulfate to form nucleated potassium sulfate and adsorb gaseous KCl. Agglomeration is more favorable when fuel ash contains a high fraction of low-melting point compounds (K, Na) and a low fraction of high-melting point compounds (Ca, Mg) [81]. In addition, the initial fuel ash composition near the eutectic composition of the low melting point appears to enhance agglomeration. The aggregates examined by scanning electron microscope showed a hollow structure with an inner region rich in K and Na, and an outer region where extensive melting was evident and the sand grains were attached by only a limited number of molten necks.

This mechanism is shown in Fig. 5. When the reaction temperature is higher than 800 °C, potassium substances will be released into the gas phase. Then complex physical transformation and chemical reaction take place. KCl vapor is the most stable potassium containing substance in the gas phase. When the temperature is higher than the melting point of KCl, the gas phase accounts for the main share. When the reaction temperature is 700–800 °C, K mainly exists in the form of KCl vapor, KCl fine particles, potassium sulfate fine particles, potassium silicate or potassium aluminum silicate [88,89]. KCl vapor nucleates uniformly to produce fine KCl particles that can also adhere to the FA particles, making FA particles more viscous. Meanwhile, potassium sulfate mainly exists in the form of fine particles. KCl vapor can also condense on nucleated potassium sulfate. Under this condition, the initial agglomeration layer is induced by non-uniform condensation of KCl vapor, and the thermal migration and diffusion of fine particles of KCl and potassium sulfate. In addition, the melting degree of the initial agglomeration layer increases with the increasing temperature. When the temperature is lower than 700 °C, KCl mainly exists in the form of fine particles which will deposit on nucleated potassium sulfate and FA particles through thermal migration and diffusion. Besides, these fine particles can be used as a binder between ashes. Under this condition, the initial agglomeration layer is mainly formed by the thermal migration and diffusion of fine particles of KCl and potassium sulfate [87].

4.3.3. Layer joint and bridge joint mechanisms

Although the formation of silicate between AAEMs and Si is the main factor of agglomeration, the growth and combination of grains are also the factors affecting agglomeration and melting. Therefore, the layer joint and bridge joint mechanisms are proposed in Fig. 6 [91].

The layer joint refers to the fact that the adjacent particles share the silicate layer to form the neck, producing large particles. In the process of biomass utilization, most of Na and K will be directly sublimated into gaseous Na/K or released into the gas phase in the form of KCl and NaCl [92]. The remaining Na and K will be transformed into silicate and sulfide with low melting point at high temperature, which will deposit or adhere to the surface of ash particles, increasing the adhesion of ash particles [93]. The bridge joint is formed by the collision between grains due to the excessive growth of grains [94], which will induce agglomeration. In the process of agglomeration induced by sulfation reaction, the excessive growth of grains leads to the formation of calcium sulfate necks. At the same time, a bridge structure is formed to connect the two particles into a weakly connected aggregate. In a laboratory scale bubble fluidized bed reactor, the product layer developed rapidly during the initial stage of sulfation and the product layer thickness was in micron scale [91], which may be responsible for the formation of interlayer connections. The bridge joint was found to be formed owing to the island overgrowth of the $CaSO_4$ crystal. The layer and bridge connections were verified in a fixed bed reactor. The orientation and mis-orientation growth of the bridge and layer connections were confirmed through transmission electron microscopy studies.

5. Strategies to mitigate the adverse impact of ash

5.1. Introduction of different gasifying agents

Traditional fuel combustion produces abundant pollutants, including SO_2 and NO_x. The gasifying agents usually take the material containing carbon as the raw material to convert fuel into combustible gas components, to improve the fuel heat utilization rate and reduce the adverse effect of ash on combustion. Gasifying agents affect the carbon

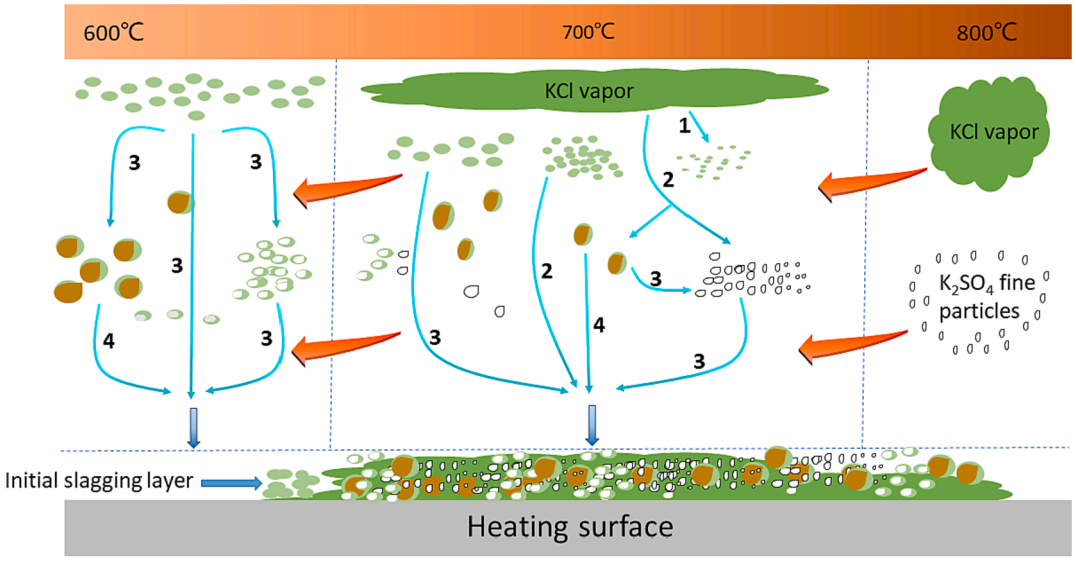

Fig. 5. Condensation mechanisms of potassium species during biomass combustion [90].

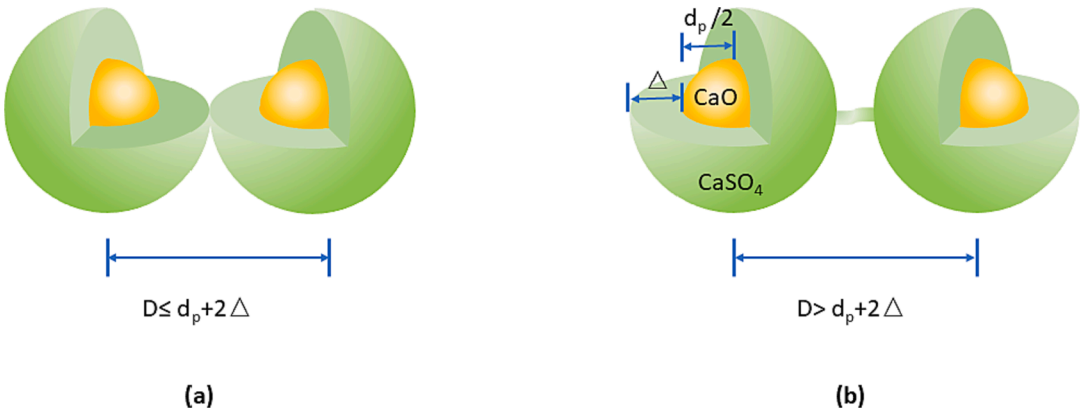

Fig. 6. The (a) layer joint and (b) bridge joint mechanisms of agglomeration [91].

conversion efficiency, the composition and heating value of product gas, and the physical and chemical properties of gasification biochar. The most common gasifying agent in CLG is H_2O, CO_2 or a mixture of both, while CO_2 and H_2O lead to different char gasification kinetics [95]. Char gasification under CO_2 atmosphere mainly generates micropores in the char matrix, whereas H_2O favors the formation of mesopores. This could result in different rates of char gasification and thus the release of ash components from char, leading to different concentrations of ash compounds in the reacting environment. As the interaction between OCs and ash is closely associated with the concentration of ash components, different reaction rates can be expected. Thus, the type of gasifying agents could lead to various extents of interaction between OCs and ash components.

5.1.1. General minerals

Some ash minerals can lead to various problems (e.g., bed sintering, bed agglomeration) in the combustor/gasifier, whereas other minerals, including Ca, K and Na, will greatly catalyze the char gasification [96]. However, the use of CO_2, H_2O or a mixture of both has shown little effect on the speciation of ash minerals. Taking Chinese bituminous coal ash as an example, it was found the main phases in ash (i.e., quartz and hematite) were kept the same and small changes were among anhydrite, cristobalite and mullite. However, the formation of cristobalite from quartz in the coal ash was substantially enhanced with the variation of temperature [97]. Another finding is the synergistic effect of calcium carbonate on char gasification with the mixture of H_2O and CO_2 [98]. As the carbonate was decomposed to CaO on the surface of coal, the oxide acts as a role of simultaneously attracting H_2O and CO_2. This then accelerates the reaction of carbon with H_2O and CO_2, demonstrating higher char gasification rate. Similarly, the combined SiO_2-Al_2O_3 phase of ash exhibited a synergistic effect on the reaction between CO and Fe_2O_3. Calculation based on density function theory suggested different frontier orbital energy as a result of the synergy to promote the reaction between CO and Fe_2O_3 [99].

5.1.2. Sulfur

Gas-phase sulfur evolution largely depends on the gas composition in the reacting environment. The formation of carbonyl sulfide can be promoted by CO at a wide temperature range, while this is also observed with CO_2 at temperatures higher than 600 °C. Nevertheless, when the reacting temperature is lower than 600 °C, CO_2 inhibits the evolution of sulfur-containing gases, which is the same case for CH_4. However, CH_4 can promote the formation of H_2S at temperature above 800 °C. H_2 can improve the formation of H_2S and inhibit the formation of other sulfurous gases [100]. Using H_2O as gasification agent, favorable intermediate conformations were introduced immediately, which has advantageous effect on sulfur binding, whereas CO_2 agent could weaken sulfur-CaO surface bonds, thus lessening the sulfur retention [101]. In the case of CLC/CLG process, there are some research activities focusing on the sulfur-OC interaction, including theoretical studies based on thermodynamics simulations with gaseous fuels and gaseous sulfur [102,103]. Ni-based OC is one of the most easily deactivated OCs because the formed NiS_x phase could cover the OC surface and thus lower the reactivity of OC [104,105]. Cu-based OC can be deactivated caused by the formation of Cu_2S [106,107]. Fe-based OC showed a resistant property against sulfur in some studies [108,109], but could form FeS in the other research [110]. Nonetheless, further studies indicated that the formation rate of FeS can be slowed down under CO_2-rich environment [111]. Additionally, CO_2 facilitated more SO_2 release with less sulfur transfer to OC [111].

5.1.3. Alkalis

In biomass fuels and municipal wastes, alkali (especially K and Na) content could be high. The alkali can catalyze the char gasification and thus lead to faster biomass conversion. Nevertheless, the high alkali content is also a cause for bed agglomeration in fluidized bed combustion. The impregnation of K^+ or Na^+ in an ilmenite OC has shown great improvement on the activity with CO [112]. However, the release behavior of K and Na was not sensitive to gasification agents and Ca release was promoted with more H_2O in the reaction atmosphere [113]. Since biomass fuels are widely applied towards negative CO_2 emissions through biomass-based CLC/CLG, K and Na in ash have been intensively investigated in recent years. Fig. 7 depicts different mechanisms of agglomerate formation with K and Na. When steam was used as gasification agent, its increasing concentration in the reaction environment had a positive effect on the release of K, which may be ascribed to facilitated conversion of K_2CO_3 to KOH (g) [114]. In this case, more gas phase alkalis were detected in the CLC/CLG process with straw pellets biomass fuel. However, most of alkalis were retained in the LD-slag OC. Different behaviors of K and Na have been revealed to lead to bed agglomeration using a braunite manganese ore as OC [115]. K exhibits earlier onset of agglomeration and defluidization as compared to Na. In addition, K and Na presented different mechanisms of agglomerates formation. As shown in Fig. 7, K tends to react with Fe and Mn in the braunite and then led to molten-derived agglomeration. On the contrary, Na did not react with braunite, but firstly led to sticky layer on the particles and then the sticky-layer derived agglomeration [115].

5.2. Pretreatment of feedstocks

5.2.1. Removing the components causing agglomeration

As a common phenomenon, agglomeration seriously affects the efficient utilization of biomass during chemical looping gasification [116,117]. In order to mitigate the agglomeration, the pretreatment using water washing, pickling, etc., has been conducted to remove certain ash components (e.g., K, Ca, Mg, Na, P, Si, S, Cl) in biomass

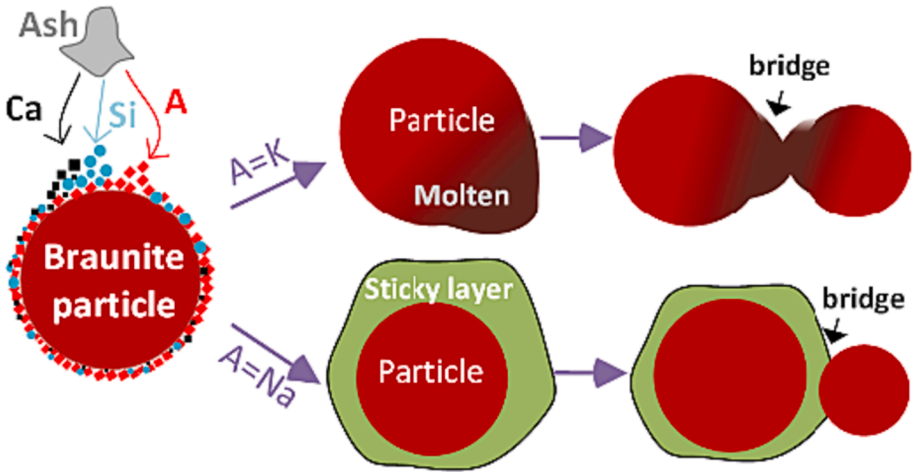

Fig. 7. Different mechanisms of agglomerate formation with K and Na.

[118–120].

Water washing refers to rinsing, soaking and stirring biomass with water for a specific time to achieve ash removal. Compared with raw biomass, the ash melting point of the washed biomass is higher, while the possibility of scaling in the reactor is less [121]. Water washing can effectively remove the ash from biomass and significantly improve the ash resistance against melting [122]. In order to investigate the effect of ash removal by water washing, the conditions in water washing have been extensively explored. Generally, the ash removal rate slightly changed with the increase of temperature [122]. Washing effectively reduced the contents of N, Cl, Ca, Mg and K in sorghum [123]. Particularly, the increase of applied water led to a reduced alkali content in ash. The removal of S, K and P in cassava straw can be improved by prolonging the washing time [124], whereas the temperature of water washing had a significant impact on the removal rate of ash in biomass [125]. Besides, the ash removal rate increased dramatically with the increase of water temperature, resulting in a distinct decrease of K and SiO_2 contents in six types of biomass [126].

However, some studies indicate that water washing can only remove the majority of soluble salts but few insoluble salts in biomass ash [127,128]. Generally, the effect of insoluble salts in biomass on agglomeration cannot be ignored. Compared with water washing, pickling can effectively remove the insoluble salts. Pickling refers to washing biomass with a certain concentration of acid solutions (e.g., nitric acid, sulfuric acid, hydrofluoric acid and hydrochloric acid) [129]. Pickling by HCl, HF and HCl + HF as agents can remarkably remove AAEMs in rape straw, especially with HCl [130]. Specifically, sulfuric acid could effectively remove 97.3 % of AAEMs, 98.4 % of chlorine and 88.8 % of phosphorus [131]. On the contrary, only 6.8 % of AAEMs and 88.0 % of chloride were removed after water washing. Furthermore, the agglomeration and slagging rate were substantially decreased after pickling pretreatment. In addition, nitric acid pickling achieved 95 % removal of AAEMs [125,132]. After nitric acid pickling, the agglomeration of pickling sample was slighter, and the grain size of main compounds was smaller than that of the original sample.

In addition to water washing and pickling, the ash in biomass can be removed by chemical fractionation, ultrasonic pretreatment and demineralization pretreatment. Chemical fractionation is a method of gradually separating components from biomass [133]. The first step is to soak the fuel in water and dissolve water-soluble compounds, such as alkali metal salts. In the second step, organically associated sodium, calcium and magnesium are replaced by ammonium ions and released into the liquid phase. In the third step, acid soluble compounds, such as carbonate and sulfate, are removed by hydrochloric acid. Alkali compounds that can affect the carbon deposition and ash agglomeration are easily leached by water and separated for analysis. Unextracted compounds by these two solvents are considered inert during combustion and will not significantly affect the combustion behavior. Ultrasonic pretreatment is a new method for material pretreatment with a frequency between 20 kHz and 1 MHz [134]. Ultrasonic pretreatment drastically reduced S and other ash components in municipal solid waste [135], effectively reducing the vulcanization process. Demineralization pretreatment can be achieved by uniformly stirring in an autoclave reactor with acetic acid solution and crude biomass [136], during which AAEMs, Cl, S and P can be removed from biomass to mitigate the emission of fine particles.

5.2.2. *Replacing the elements causing agglomeration*

Although a few AAEMs have certain effects on agglomeration in CLG, other AAEMs with catalytic effect are also removed along with the process of ash removal from biomass. Actually, the substitution of exogenous AAEMs for their inherent AAEMs in biomass can effectively maintain its catalytic effect and reduce its impact on agglomeration [67].

AAEMs are often added by impregnation. Impregnation method is to immerse biomass in a salt solution containing specific metal ions, and then the metal ions in the solution are penetrated into the internal structure of biomass through capillary pressure [14]. The existing form of alkali metal will affect its catalytic reactivity. For instance, the effect of acetate metal salt on reaction temperature and product is significantly greater than that of chloride metal salt [131]. During pyrolysis, addition of acetate metal could divide cellulose pyrolysis into two stages and increase H_2 content in the pyrolysis gas, while introduction of chloride metal reduced H_2 yield [66]. Due to slight agglomeration, gasification efficiency in the presence of calcium acetate was higher than that of calcium chloride where Cl played an important role in agglomeration [71]. Although AAEMs in biomass are the main cause of agglomeration, a single metal addition in biomass will promote the reaction and mitigate the agglomeration after the removal of original AAEMs. For example, a high content of CaO would react with CO_2 in the reaction gas to form a layer of $CaCO_3$ film that covered the biomass surface to mitigate agglomeration [137]. Furthermore, the gasification efficiency of Mg-loaded biomass was increased by elevating Mg concentration, however, the grain growth rate was still relatively slow. When 6.6 times of original Mg amount was added, efficient gasification without severe agglomeration could be expected [64].

5.3. *Recycle valuable components from OCs*

Due to attrition as well as discharge along with ash, there is a loss of OC during the circulation in CLC system. Thus, a makeup of fresh OC is needed, which contributes to additional OC cost for CLC system, e.g., an

estimated cost of 175–225 €/ton in the case of ilmenite and manganese ore [138]. The cost will be much higher in the case of synthetic OC which usually involves more expensive precursors, inert support or other chemicals. As stated before, it is inevitable that OC can interact with ash components, especially S, K and Na. In the case of long-time exposure to alkalis or sulfur in the fuel reactor, the OC reactivity may decrease and become unsuitable for CLG process. These OCs must be discharged from the fuel reactor, thereby increasing the system cost. As depicted in Fig. 8, metals combined with spent OCs can be recycled for industrial use or reproduction of OCs in CLG or CLC to lower/compensate this induced cost. Leaching with water or strong acid is a common technique to recover valuable metals (e.g., vanadium) or Fe, Cu, Mn for fabrication of synthetic OCs or modification of natural ores with enhanced properties.

5.3.1. Leaching valuable metals for industrial use

Leaching useful metals from fuel ash was studied to some extent. Removal of calcium was reported to increase the recoverability of aluminum from coal ash [139]. Mineral carbonation reaction can decrease the leachability of Zn, Cu, Pb, Ni, As, Hg, Cd, Cr, Cl, and SO_4^{2-}, as well as reduce the solvent pH from 12 to about 9 [140]. Diluted acetic acid can leach out K but retain Ca in biomass [141]. Thus, there will be more possibilities and opportunities by integrating leaching technology into CLP.

During CLC/CLG process, OC can interact with ash to accumulate value-added metals after a long-term operation. Some of the accumulated elements are extractable via water/acid leaching. Preliminary research work has been done to recover vanadium from LD-slag OC from CLC in a 12 MW_{th} boiler located at Chalmers University of Technology. Continuous leaching was examined using sulphuric acid with or without microwave treatment. After microwave treatment, leaching efficiency was elevated from 22.1 % to 49.1 %. This opens up the possible reutilization of value-added elements from industrial process and sustainable disposal of OCs from CLP.

5.3.2. Leaching active metals for OC re-synthesis

In general, active metals (e.g., Fe, Mn, Cu) in OC are more leachable than the ash components, such as quartz, corundum and aluminosilicates, thus there are possibilities to recover useful metals (e.g., Fe, Cu, Mn) and semi-metal oxides (e.g., silica) via OC leaching. Strong acid is used to leach these metals for promising reuse in OC synthesis for CLC/CLG process. Nonetheless, limited research has been implemented owing to appropriate selection of effective leaching agent for recovery of valuable components from the mineral matrix of spent OC. Meanwhile, the property of leaching agent is crucial for the re-synthesis of OC. For example, the precipitation of active metal oxide should be possible during the pH swing process [142]. Copper leaching with HNO_3 was previously investigated for the spent Cu-Al OC in a 10 kW_{th} CLC unit to reveal the feasibility for the synthesis of new OC [143]. Residual alumina after the leaching of Cu-Al OC can be recycled to produce high-strength ceramic spheres that can be used as high-performance filters for industrial process. Similarly, the feasibility was also confirmed for a C28 calcium manganite-based OC prepared from spray drying [144].

5.4. Novel design of OCs

Functionality of OC is crucial for the success of CLG process. In order to promote the development of CLG technology, structural and compositional optimization of OC is essential to remarkably enhance the activity and durability of OC.

5.4.1. Structural optimization

Grain growth will block the pore structure of OC during reactions, which is one of the main causes for bed agglomeration and OC deactivation. In addition, a higher temperature will lead to the collapse of pore structure of OC, decreasing the specific surface area of OC and generating lower melting point compounds. This will degrade the reaction performance of OC. Construction of OC with developed pore structure and high structural stability is an effective solution to agglomeration in CLG.

Three dimensional ordered macroporous OC (3DOM OC) is a kind of macroporous OC with pore diameter above 50 nm. Because of its unique structure with uniform macropore diameter, ordered arrangement of pores and small window communication between macropores, an internal cross-linked three-dimensional macropore network can be formed, leading to higher specific surface area and larger pore volume. The commonly used colloidal microsphere materials mainly include polystyrene, polymethylmethacrylate and SiO_2 [145,146]. In addition, the preparation methods of microspheres include suspension polymerization, lotion polymerization, dispersion polymerization, precipitation polymerization, soap free lotion polymerization, seed expansion and distillation precipitation polymerization [142,147]. Colloidal crystal templates usually combine microspheres by self-assembly (e.g., centrifugation, gravity sedimentation, vertical deposition, etc.) [148]. 3DOM OC has been revealed to possess a higher porosity and order according to scanning electron microscope, transmission electron microscope and photonic stop band properties [149]. As compared to pure Fe_2O_3 OC, the as-prepared 3DOM Fe_2O_3 OC exhibited an increase of 7.1 % and 0.29

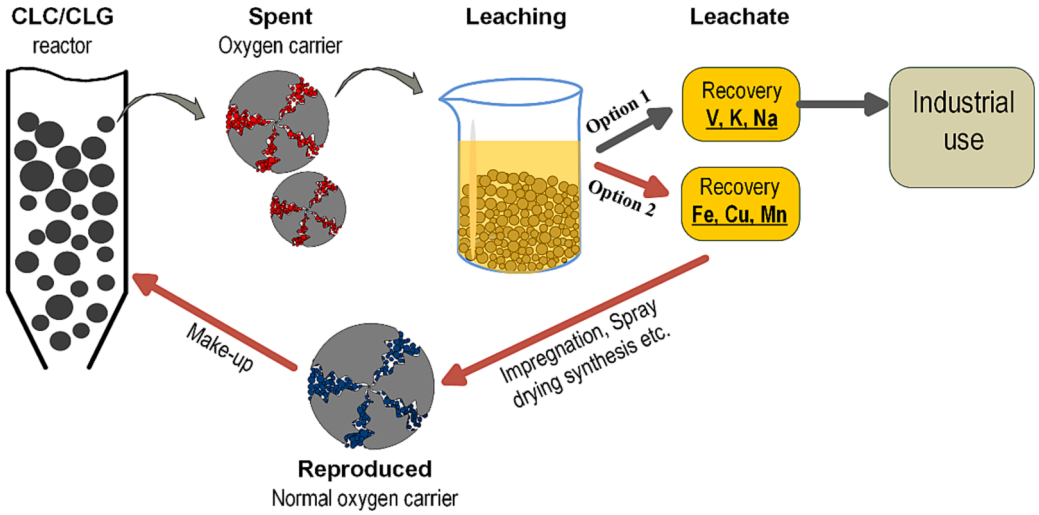

Fig. 8. Recycle and reuse routes of spent OCs.

%/min for the maximum weight loss and the maximum weight loss rate, respectively, in gasification stage [150].

Molecular sieves, typical ordered mesoporous materials, demonstrate high specific surface area. Besides, their mesoporous structure can enhance the dispersion of active metals and increase the diffusion of reactants [151]. Molecular sieve materials include HY, ZSM-5, SAPO-34, MCM-41 and 5A, etc. [152–154]. OC prepared by molecular sieves could exhibit high activity, high selectivity and high stability. For instance, 5Ni/MCM-41 significantly improved H_2 and CO production from gasification of cassava roots with conversion efficiency of carbon and hydrogen of 80.17 % and 27.39 %, respectively, and 10 wt% decrease of liquid yield [155]. Ni/SBA-16 showed a stronger reduction, oxidation and anti-agglomeration ability [156].

Stability and reusability of OCs should be improved to inhibit the leaching and agglomeration of noble metal OCs. A layer of shell was coated on the pre-synthesized nanoparticles to construct OC with core–shell structure [157], which had an obvious inhibitory effect on metal sintering and agglomeration [158]. Methods to construct a core–shell structure mainly include deposition precipitation and one-pot method [158–160]. Ni@SiO_2 prepared by deposition precipitation was found to demonstrate high specific surface area, small particle size and uniform metal dispersion, and the highest long-term stability [159]. Three-layer core–shell structure is further developed to strengthen the resistance to agglomeration under the action of double inert components. For example, Ni-SiO_2@CeO showed stronger resistance to sintering and agglomeration of Ni particles as compared with Ni@SiO_2 and Ni@CeO [160].

5.4.2. Compositional optimization

Previously, monometallic OCs (e.g., Fe_2O_3, CuO, NiO_2) have been widely applied in CLG. Due to their disadvantages of poor cyclic performance and serious agglomeration, bimetallic or polymetallic OCs have been extensively prepared and examined, such as loading inert carriers, the preparation of composite OCs and mixed OCs.

At present, there are four common methods to load active components on inert carriers, i.e., mechanical mixing, co-precipitation, impregnation and sol–gel [161,162]. Mechanical mixing method is simple but the distribution of active components is uneven. In spite of complete distribution of active components on the surface of inert carrier, impregnation has drawbacks in terms of long synthesis time and uncontrollable impregnation. Co-precipitation and sol–gel are advantageous methods for convenient OC preparation with superior loading effect. So far, common inert carriers are La_2O_3, CeO_2, Al_2O_3, SiO_2, MgO, ZnO, $MgAl_2O_3$, bentonite, limonite and kaolin [163–165]. The existence of inert carrier can effectively improve the dispersion of active components and mitigate the sintering problem. Some inert carriers also have a certain catalytic effect on the reaction. For example, MgO showed catalytic effect on tar removal [166,167]. The redox activity of ZnO is low, but it has the potential to enhance syngas production [165]. Fe_2O_3/Al_2O_3 OC remained stable after ten redox cycles of CLG in terms of chemical properties, crystal size, specific surface area and pore structure [161,162]. After CaO was loaded on Fe_2O_3 OC, CaO could form a film to cover the surface of OC at high temperature, agglomeration was inhibited to a certain extent in spite of a decrease in reaction activity of OC [168]. In addition, when composite oxide was loaded on inert carrier, OC containing inert carrier suggested a better recyclability [169]. Moreover, the addition of MgO improved the oxygen release capacity of $Ca_2Fe_2O_5$ [42]. Meanwhile, loading active component on MgO increased the melting point of the reduced OC and inhibited the growth of $Ca_2Fe_2O_5$ crystal size, leading to mitigated agglomeration.

Two or more active metal oxides or nitrates can be mixed and calcined to prepare bimetallic or polymetallic OCs, such as $NiFe_2O_4$, $CuFe_2O_4$, $MnFe_2O_4$ and $CoFeAlO_x$ [20,170,171]. $NiFe_2O_4$ OC was prepared using high-temperature ball-milling assisted solid-state reaction [172] and showed stronger reaction performance and better stability than NiO and Fe_2O_3 after five redox cycles. Through thermogravimetric analysis of $CuFe_2O_4$, the reaction superiority and recoverability of $CuFe_2O_4$ was proved to be stronger after reaction [170]. $CoFeAlO_x$ is an OC during oxidative coupling of methane, in which the active phase of CoFe alloy and the parent spinel carrier were evenly mixed into the solid. Meanwhile, the dissolved CoFe alloy can be embedded in the scaffold of carrier after reduction [173]. After 20 redox cycles, it showed high reaction performance and excellent stability, indicating that controllable melting can significantly improve the high-temperature redox performance of OC.

Doped OC demonstrates changes in crystal structure by doping elements to form more oxygen vacancies, leading to improvement of activity and crystal melting point [25]. Co was doped into $Ca_2Fe_2O_5$ to form $Ca_2Fe_{1.8}Co_{0.2}O_5$[25], which maintained high reaction performance and complete crystal structure after 10 redox cycles. Perovskite OC is also a kind of doped OC [174], which has strong lattice oxygen transport ability [175]. Especially, the alkaline earth metal doped with perovskite OC can effectively catalyze the reaction and avoid agglomeration during reaction [176]. Different types of perovskite OCs have been prepared by adjusting the ratio of $Ba(NO_3)_2$, $Sr(NO_3)_2{\cdot}4H_2O$, $CO(NO_3)_2{\cdot}6H_2O$ and $Fe(NO_3)_3{\cdot}9H_2O$ [177]. $Ba_{0.5}Sr_{0.5}Co_{0.8}Fe_{0.2}O_{3-\delta}$ was found to be stable with only slight agglomeration after several redox cycles.

6. Conclusions

Influence of ash content in biomass and waste steams on CLP has been holistically summarized and analyzed. Certain elements in ash (e.g., Ca and Fe) can act as active OCs to enhance the performance of CLP to a certain extent. However, the majority of ash compositions and their physical states have adverse effects on CLP to deactivate OCs. AAEMs, such as K, Na, Ca and Mg, are converted into low melting point substances at high temperature, resulting in particle agglomeration. In addition, alkali-rich elements released during biomass combustion tend to react with silicates, forming alkali-silicates and alkali-aluminosilicates that gradually accumulate as condensates within molten particles. Grain growth and aggregation also contribute to agglomeration and melting. To mitigate detrimental effects of ash components in biomass fuels, various strategies can be deployed. Different gasifying agents can be introduced to induce synergy with general minerals, gaseous sulfur and gaseous alkalis. Additionally, ash in biomass can be removed through washing, chemical fractionation, ultrasonic pretreatment, and demineralization pretreatment. Importantly, removal of catalytic AAEMs should be avoided, while additional exogenous AAEMs can preserve their catalytic effects. Moreover, valuable and active metals can be leached out and recycled from spent OC for industrial use and re-synthesis of new OC. Constructing OCs with well-developed pore structure and high stability offers an effective solution to address the agglomeration issue. Besides, novel bimetallic or polymetallic OCs shall be designed to enhance reactivity and crystal melting points. Eventually, energy efficiency of biomass fuel would be remarkably enhanced by addressing these challenges posed by ash to advance CLP-based sustainable energy system.

Declaration of Competing Interest

The authors declare the following financial interests/personal relationships which may be considered as potential competing interests: Chao He reports was provided by Research Council of Finland. Zhifeng Hu reports was provided by Natural Science Foundation of Guangdong Province. Zhifeng Hu reports was provided by Department of Education of Guangdong Province.

Data availability

Data will be made available on request.

Acknowledgements

C. He acknowledges the Academy Research Fellowship and its related research project funded by Research Council of Finland (decision numbers: 341052, 346578). Z. Hu is grateful for Guangdong Basic and Applied Basic Research Foundation (No. 2022A1515010738) and Department of Education of Guangdong Province (No. 2021KTSCX011) for the support. B. Bhui is acknowledged for her initial comments on this work.

References

[1] C.-C. Cormos, Techno-economic evaluations of copper-based chemical looping air separation system for oxy-combustion and gasification power plants with carbon capture, Energies 11 (2018).
[2] M. Luo, Y. Yi, C. Wang, K. Liu, J. Pan, Q. Wang, Energy and exergy analysis of power generation systems with chemical looping combustion of coal, Chem Eng Technol 41 (2018) 776–787.
[3] L. Liu, Z. Li, S. Wu, D. Li, N. Cai, Conversion characteristics of lignite and petroleum coke in chemical looping combustion coupled with an annular carbon stripper, Fuel Process Technol 213 (2021).
[4] I. Gogolev, T. Pikkarainen, J. Kauppinen, C. Linderholm, B.-M. Steenari, A. Lyngfelt, Investigation of biomass alkali release in a dual circulating fluidized bed chemical looping combustion system, Fuel 297 (2021).
[5] X. Niu, L. Shen, H. Gu, S. Jiang, J. Xiao, Characteristics of hematite and fly ash during chemical looping combustion of sewage sludge, Chem Eng J 268 (2015) 236–244.
[6] H. Leion, X. Zhan, V. Frick, Determining CLOU reaction kinetics for combined oxygen carriers-discussing the experimental methods, Energ. Technol. 4 (2016) 1247–1253.
[7] C. Saha, B. Roy, S. Bhattacharya, Chemical looping combustion of Victorian brown coal using NiO oxygen carrier, Int. J. Hydrogen Energy 36 (2011) 3253–3259.
[8] X. Zhao, H. Zhou, V.S. Sikarwar, M. Zhao, A.-H.-A. Park, P.S. Fennell, L. Shen, L.-S. Fan, Biomass-based chemical looping technologies: the good, the bad and the future, Energ. Environ. Sci. 10 (2017) 1885–1910.
[9] I. Staničić, M. Hanning, R. Deniz, T. Mattisson, R. Backman, H. Leion, Interaction of oxygen carriers with common biomass ash components, Fuel Process Technol 200 (2020).
[10] Z. Miao, E. Jiang, Z. Hu, Review of agglomeration in biomass chemical looping technology, Fuel 309 (2022).
[11] S. Du, H. Yang, K. Qian, X. Wang, H. Chen, Fusion and transformation properties of the inorganic components in biomass ash, Fuel 117 (2014) 1281–1287.
[12] X.-M. Li, H. Zhang, M.-J. Liu, L.-F. Zhi, J. Bai, Z.-Q. Bai, W. Li, Investigation of coal-biomass interaction during co-pyrolysis by char separation and its effect on coal char structure and gasification reactivity with CO_2, J. Fuel Chem. Technol. 48 (2020) 897–907.
[13] Y. Liu, X. Zhang, M. Gao, X. Hu, Q. Guo, Effect of coal ash on Fe-based oxygen carrier in coal char chemical looping gasification, Int J Chem React Eng 17 (2019).
[14] S.V. Vassilev, D. Baxter, C.G. Vassileva, An overview of the behaviour of biomass during combustion: Part II ash fusion and ash formation mechanisms of biomass types, Fuel 117 (2014) 152–183.
[15] J.-I. Baek, C.K. Ryu, J.H. Lee, T.H. Eom, J.B. Lee, H.-J. Ryu, J. Ryu, J. Yi, The effects of using structurally less-stable raw materials for the support of a spray-dried oxygen carrier with high NiO content, Fuel 102 (2012) 106–114.
[16] M.M. Azis, H. Leion, E. Jerndal, B.M. Steenari, T. Mattisson, A. Lyngfelt, The effect of bituminous and lignite ash on the performance of ilmenite as oxygen carrier in chemical-looping combustion, Chem Eng Technol 36 (2013) 1460–1468.
[17] A. Rubel, Y. Zhang, K. Liu, J. Neathery, Effect of ash on oxygen carriers for the application of chemical looping combustion to a high carbon char, Oil & Gas Science and Technology – Revue d'IFP Energies Nouvelles 66 (2011) 291–300.
[18] S.V. Vassilev, D. Baxter, C.G. Vassileva, An overview of the behaviour of biomass during combustion: Part I phase-mineral transformations of organic and inorganic matter, Fuel 112 (2013) 391–449.
[19] Y. Wang, X. Tian, H. Zhao, K. Liu, The use of a low-cost oxygen carrier prepared from red mud and copper ore for in situ gasification chemical looping combustion of coal, Fuel Process Technol 205 (2020).
[20] B. Wang, R. Yan, H. Zhao, Y. Zheng, Z. Liu, C. Zheng, Investigation of chemical looping combustion of coal with $CuFe_2O_4$ oxygen carrier, Energ Fuel 25 (2011) 3344–3354.
[21] R. Gong, C. Qin, D. He, L. Tan, J. Ran, Oxygen uncoupling of cu-based oxygen carrier with the presence of coal ash in chemical looping process, Energ Fuel 32 (2018) 7708–7717.
[22] J. Bao, Z. Li, N. Cai, Interaction between iron-based oxygen carrier and four coal ashes during chemical looping combustion, Appl. Energy 115 (2014) 549–558.
[23] C. Dan, Y. Qi, G. Ben, Z. Yong, Z. Jun, Carbothermal interaction between Cu-based oxygen carrier and ash minerals in the chemical looping gasification of coal and biomass, J. Fuel Chem. Technol 48 (2020) 19–27.
[24] J. Dai, K.J. Whitty, Predicting and alleviating coal ash-induced deactivation of CuO as an oxygen carrier for chemical looping with oxygen uncoupling, Fuel 241 (2019) 1214–1222.
[25] G. Liu, Y. Liao, Y. Wu, X. Ma, Reactivity of Co-doped $Ca_2Fe_2O_5$ brownmillerite oxides as oxygen carriers for microalgae chemical looping gasification, Int. J. Hydrogen Energy 44 (2019) 2546–2559.
[26] F. Xu, X. Xing, S. Gao, W. Zhang, L. Zhu, Y. Wang, J. Chen, H. Chen, Y. Zhu, Direct chemical looping gasification of pine sawdust using Fe_2O_3-rich sludge ash as an oxygen carrier: thermal conversion characteristics, product distributions, and gasification performances, Fuel 304 (2021).
[27] K. Yin, H. Wang, A. Veksha, X. Dou, D.K.B. Mohamed, S. Heberlein, G. Liu, W. Chen, G. Lisak, Oxygen carriers from incineration bottom ash for chemical looping combustion of syngas: effect of composition on combustion efficiency, Chem Eng J 405 (2021).
[28] K. Wang, Z. An, F. Wang, W. Liang, C. Wang, Q. Guo, Y. Liu, G. Yue, Effect of ash on the performance of iron-based oxygen carrier in the chemical looping gasification of municipal sludge, Energy 231 (2021).
[29] S. Zhang, H. Gu, J. Zhao, L. Shen, L. Wang, Development of iron ore oxygen carrier modified with biomass ash for chemical looping combustion, Energy 186 (2019).
[30] J. Ma, X. Tian, H. Zhao, J. Ma, C. Zheng, Effect of coal ash on the performance of $CuO@TiO_2$-Al_2O_3 in chemical looping with oxygen uncoupling, Fuel Process. Technol. 221 (2021).
[31] A. Cuadrat, A. Abad, F. García-Labiano, P. Gayán, L.F. de Diego, J. Adánez, Ilmenite as oxygen carrier in a chemical looping combustion system with coal, Energy Procedia 4 (2011) 362–369.
[32] H. Gu, L. Shen, Z. Zhong, Y. Zhou, W. Liu, X. Niu, H. Ge, S. Jiang, L. Wang, Interaction between biomass ash and iron ore oxygen carrier during chemical looping combustion, Chem Eng J 277 (2015) 70–78.
[33] X. Huang, M. Fan, X. Wang, Y. Wang, M.D. Argyle, Y. Zhu, A cost-effective approach to realization of the efficient methane chemical-looping combustion by using coal fly ash as a support for oxygen carrier, Appl. Energy 230 (2018) 393–402.
[34] Z. Xu, H. Zhao, Y. Wei, C. Zheng, Self-assembly template combustion synthesis of a core–shell $CuO@TiO_2$–Al_2O_3 hierarchical structure as an oxygen carrier for the chemical-looping processes, Combust. Flame 162 (2015) 3030–3045.
[35] Y. Liu, S. Wang, R. Lohmann, N. Yu, C. Zhang, Y. Gao, J. Zhao, L. Ma, Source apportionment of gaseous and particulate PAHs from traffic emission using tunnel measurements in Shanghai, China, Atmos. Environ. 107 (2015) 129–136.
[36] Z. Zhang, M. Tang, Z. Yang, J. Ma, L. Liu, B. Shen, SO_2 and NO emissions during combustion of high-alkali coal over a wide temperature range: effect of Na species and contents, Fuel 309 (2022).
[37] L. Aisyah, P.J. Ashman, C.W. Kwong, Performance of coal fly-ash based oxygen carrier for the chemical looping combustion of synthesis gas, Appl. Energy 109 (2013) 44–50.
[38] A. Skulimowska, L. Di Felice, N. Kamińska-Pietrzak, A. Celińska, M. Pławecka, J. Hercog, M. Krauz, A. Aranda, Chemical looping with oxygen uncoupling (CLOU) and chemical looping combustion (CLC) using copper-enriched oxygen carriers supported on fly ash, Fuel Process Technol 168 (2017) 123–130.
[39] G. Wei, H. Wang, W. Zhao, Z. Huang, Q. Yi, F. He, K. Zhao, A. Zheng, J. Meng, Z. Deng, J. Chen, Z. Zhao, H. Li, Synthesis gas production from chemical looping gasification of lignite by using hematite as oxygen carrier, Energ. Conver. Manage. 185 (2019) 774–782.
[40] H. Gu, L. Shen, Z. Zhong, X. Niu, W. Liu, H. Ge, S. Jiang, L. Wang, Cement/CaO-modified iron ore as oxygen carrier for chemical looping combustion of coal, Appl. Energy 157 (2015) 314–322.
[41] Z. Sun, S. Chen, C.K. Russell, J. Hu, A.H. Rony, G. Tan, A. Chen, L. Duan, J. Boman, J. Tang, T. Chien, M. Fan, W. Xiang, Improvement of H_2-rich gas production with tar abatement from pine wood conversion over bi-functional $Ca_2Fe_2O_5$ catalyst: investigation of inner-looping redox reaction and promoting mechanisms, Appl. Energy 212 (2018) 931–943.
[42] G. Liu, Y. Liao, Y. Wu, X. Ma, Enhancement of $Ca_2Fe_2O_5$ oxygen carrier through Mg/Al/Zn oxide support for biomass chemical looping gasification, Energ. Conver. Manage. 195 (2019) 262–273.
[43] L. Protasova, F. Snijkers, Recent developments in oxygen carrier materials for hydrogen production via chemical looping processes, Fuel 181 (2016) 75–93.
[44] R. Siriwardane, J. Riley, H. Tian, G. Richards, Chemical looping coal gasification with calcium ferrite and barium ferrite via solid–solid reactions, Appl. Energy 165 (2016) 952–966.
[45] Y. Liu, X. Zhang, Effect of coal ash on fe-based oxygen carrier in coal char chemical looping gasification, Int J Chem React Eng 17 (2019), 20180270.
[46] D. Yilmaz, H. Leion, Interaction of iron oxygen carriers and alkaline salts present in biomass-derived ash, Energ Fuel 34 (2020) 11143–11153.
[47] X.-D. Chen, L.-X. Kong, J. Bai, Z.-Q. Bai, W. Li, Effect of Na_2O on mineral transformation of coal ash under high temperature gasification condition, J. Fuel Chem. Technol. 44 (2016) 263–272.
[48] L. Mu, L. Zhao, L. Liu, H. Yin, Elemental distribution and mineralogical composition of ash deposits in a large-scale wastewater incineration plant: a case study, Ind. Eng. Chem. Res. 51 (2012) 8684–8694.
[49] D. Lindberg, R. Backman, P. Chartrand, M. Hupa, Towards a comprehensive thermodynamic database for ash-forming elements in biomass and waste combustion — current situation and future developments, Fuel Process. Technol. 105 (2013) 129–141.
[50] A. Mlonka-Mędrala, A. Magdziarz, M. Gajek, K. Nowińska, W. Nowak, Alkali metals association in biomass and their impact on ash melting behaviour, Fuel 261 (2020).

[51] L. Yu, W. Zhou, Z. Luo, H. Wang, W. Liu, K. Yin, Developing Oxygen Carriers for Chemical Looping Biomass Processing: Challenges and Opportunities 4 (2020), 2000099.

[52] B. Bhui, P. v,, Chemical looping based co-combustion of high ash Indian coal and rice straw operating under CO_2 in-situ gasification mode, J Energy Inst 94 (2021) 176–190.

[53] P. Moldenhauer, S. Sundqvist, T. Mattisson, C. Linderholm, Chemical-looping combustion of synthetic biomass-volatiles with manganese-ore oxygen carriers, Int. J. Greenhouse Gas Control 71 (2018) 239–252.

[54] K. Kim, S. Yang, J.-I. Baek, C.K. Ryu, M. Choi, Y. He, K. Shin, G. Lee, New fabrication of mixed oxygen carrier for CLC: Sludge and scale from a power plant, Fuel 111 (2013) 496–504.

[55] Q. Chen, S. Hu, Q. Xu, S. Su, Y. Wang, K. Xu, L. He, J. Xiang, Steam synergic effect on oxygen carrier performance and WGS promotion ability of iron-oxides, Energy 215 (2021).

[56] T. Xu, C. Jiang, X. Wang, B. Xiao, Bio-oil chemical looping reforming coupled with water splitting for hydrogen and syngas coproduction: effect of supports on the performance of Ni-Fe bimetallic oxygen carriers, Energ. Conver. Manage. 244 (2021).

[57] J. Zhang, T. He, Z. Wang, M. Zhu, K. Zhang, B. Li, J. Wu, The search of proper oxygen carriers for chemical looping partial oxidation of carbon, Appl. Energy 190 (2017) 1119–1125.

[58] M. Pishahang, Y. Larring, J. Adánez, P. Gayán, M. Sunding, Fe_2O_3–Al_2O_3 oxygen carrier materials for chemical looping combustion, a redox thermodynamic and thermogravimetric evaluation in the presence of H2S, J Therm Anal Calorim 134 (2018) 1739–1748.

[59] T. Mattisson, D. Jing, A. Lyngfelt, M. Rydén, Experimental investigation of binary and ternary combined manganese oxides for chemical-looping with oxygen uncoupling (CLOU), Fuel 164 (2016) 228–236.

[60] Q. Hong, T. Shen, P. Wang, L. Shen, L. Cheng, T. Song, Evaluation of different red muds as oxygen carriers in a fluidized bed thermogravimetric analyzer, Energ Fuel 35 (2021) 14805–14815.

[61] B. Sub Kwak, N.-K. Park, H.-J. Ryu, J.-I. Baek, M. Kang, Reduction and oxidation performance evaluation of manganese-based iron, cobalt, nickel, and copper bimetallic oxide oxygen carriers for chemical-looping combustion, Appl. Therm. Eng. 128 (2018) 1273–1281.

[62] H. Leion, A. Lyngfelt, M. Johansson, E. Jerndal, T. Mattisson, The use of ilmenite as an oxygen carrier in chemical-looping combustion, Chem. Eng. Res. Des. 86 (2008) 1017–1026.

[63] J.D. Morris, S.S. Daood, S. Chilton, W. Nimmo, Mechanisms and mitigation of agglomeration during fluidized bed combustion of biomass: a review, Fuel 230 (2018) 452–473.

[64] J. Wu, J. Lv, Y. Lin, W. Wu, H. Xin, J. Zhao, Y. Ren, M. Wang, E. Jiang, Z. Hu, Effect of Mg in rice husk on promoting reaction and causing agglomeration during chemical looping gasification, Chem Eng J 437 (2022).

[65] J. Wu, Z. Hu, Z. Miao, W. Wu, E. Jiang, Effect of alkaline earth metal Ca in rice husk during chemical looping gasification process, Fuel 299 (2021).

[66] J. Long, H. Song, X. Jun, S. Sheng, S. Lun-Shi, X. Kai, Y. Yao, Release characteristics of alkali and alkaline earth metallic species during biomass pyrolysis and steam gasification process, Bioresour Technol 116 (2012) 278–284.

[67] C. Erbel, M. Mayerhofer, P. Monkhouse, M. Gaderer, H. Spliethoff, Continuous in situ measurements of alkali species in the gasification of biomass, Proc. Combust. Inst. 34 (2013) 2331–2338.

[68] L.E. Fryda, K.D. Panopoulos, E. Kakaras, Agglomeration in fluidised bed gasification of biomass, Powder Technol. 181 (2008) 307–320.

[69] H. Namkung, L.-H. Xu, C.H. Kim, X. Yuan, T.-J. Kang, H.-T. Kim, Effect of mineral components on sintering of ash particles at low temperature fouling conditions, Fuel Process. Technol. 141 (2016) 82–92.

[70] H. Namkung, Y.-J. Lee, J.-H. Park, G.-S. Song, J.W. Choi, J.-G. Kim, S.-J. Park, J. C. Park, H.-T. Kim, Influence of herbaceous biomass ash pre-treated by alkali metal leaching on the agglomeration/sintering and corrosion behaviors, Energy 187 (2019), 115950.

[71] Y. Wu, Y. Liao, G. Liu, X. Ma, Syngas production by chemical looping gasification of biomass with steam and CaO additive, Int J Hydrogen Energ 43 (2018) 19375–19383.

[72] S.V. Vassilev, D. Baxter, L.K. Andersen, C.G. Vassileva, An overview of the chemical composition of biomass, Fuel 89 (2010) 913–933.

[73] J. Bao, Z. Li, N. Cai, Reduction kinetics of foreign-ion-promoted ilmenite using carbon monoxide (CO) for chemical looping combustion, Ind. Eng. Chem. Res. 52 (2013) 10646–10655.

[74] S.V. Vassilev, D. Baxter, L.K. Andersen, C.G. Vassileva, An overview of the composition and application of biomass ash. Part 1. Phase–mineral and chemical composition and classification, Fuel 105 (2013) 40–76.

[75] Y. Niu, H. Tan, X. Wang, Z. Liu, H. Liu, Y. Liu, T. Xu, Study on fusion characteristics of biomass ash, Bioresour Technol 101 (2010) 9373–9381.

[76] G. Dunnu, J. Maier, G. Scheffknecht, Ash fusibility and compositional data of solid recovered fuels, Fuel 89 (2010) 1534–1540.

[77] S. Leiser, M.K. Cieplik, R. Smit, Slagging behavior of straw and corn stover and the fate of potassium under entrained-flow gasification conditions, Energ Fuel 27 (2013) 318–326.

[78] E. Karampinis, D. Vamvuka, S. Sfakiotakis, P. Grammelis, G. Itskos, E. Kakaras, Comparative study of combustion properties of five energy crops and greek lignite, Energ Fuel 26 (2012) 869–878.

[79] J. Wu, H. Liang, Y. Wang, J. Zhang, Q. Zhang, J. Lv, E. Jiang, Y. Ren, Z. Hu, Effect of alkali metals and alkaline earth metals on promotion and agglomeration of Fe-based oxygen carrier during chemical looping gasification, Fuel Process Technol 250 (2023).

[80] C. Hsia, G.R.S. Pierre, L.S. Fan, Isotope study on diffusion in $CaSO_4$ formed during sorbent-flue-gas reaction, AIChE J 41 (1995) 2337–2340.

[81] F. Scala, R. Chirone, An SEM/EDX study of bed agglomerates formed during fluidized bed combustion of three biomass fuels, Biomass Bioenergy 32 (2008) 252–266.

[82] C.A. Wang, G. Li, Y. Du, Y. Yan, H. Li, D. Che, Ash deposition and sodium migration behaviors during combustion of Zhundong coals in a drop tube furnace, J. Energy Inst. 91 (2018) 251–261.

[83] S. Hu, Y. Ni, Q. Yin, J. Wang, L. Lv, K. Cen, H. Zhou, Research on element migration and ash deposition characteristics of high-alkali coal in horizontal liquid slagging cyclone furnace, Fuel 308 (2022).

[84] J. Hu, Y. Yan, Y. Song, J. Liu, F. Evrendilek, M. Buyukada, Catalytic combustions of two bamboo residues with sludge ash, CaO, and Fe_2O_3: Bioenergy, emission and ash deposition improvements, J. Clean. Prod. 270 (2020).

[85] L. Shen, Z. Gao, J. Wu, J. Xiao, Sulfur behavior in chemical looping combustion with NiO/Al2O3 oxygen carrier, Combust. Flame 157 (2010) 853–863.

[86] P. Billen, B. Creemers, J. Costa, J. Van Caneghem, C. Vandecasteele, Coating and melt induced agglomeration in a poultry litter fired fluidized bed combustor, Biomass Bioenergy 69 (2014) 71–79.

[87] X.G. Xu, S.Q. Li, G.D. Li, Q. Yao, Effect of co-firing straw with two coals on the ash deposition behavior in a down-fired pulverized coal combustor, Energy Fuel 24 (2010) 241–249.

[88] F. Scala, Characterization and Early Detection of Bed Agglomeration during the fluidized bed combustion of olive husk, (2006).

[89] R. Chirone, F. Miccio, F. Scala, Mechanism and prediction of bed agglomeration during fluidized bed combustion of a biomass fuel: Effect of the reactor scale, Chem Eng J 123 (2006) 71–80.

[90] X. Jin, J. Ye, L. Deng, D. Che, Condensation behaviors of potassium during biomass combustion, Energy Fuel 31 (2017) 2951–2958.

[91] D. Li, X. Qu, J. Li, S.W. Hong, C.-H. Jeon, Microstructural development of product layer during limestone sulfation and its relationship to agglomeration in large-scale CFB boiler, Energy 238 (2022).

[92] H. Wang, S. Guo, D. Liu, Y. Guo, D. Gao, S. Sun, A dynamic study on the impacts of water vapor and impurities on limestone calcination and CaO sulfurization processes in a microfluidized bed reactor analyzer, Energy Fuel 30 (2016) 4625–4634.

[93] C. Chen, Y. Zhuang, C. Wang, Enhancement of direct sulfation of limestone by Na2CO3 addition, Fuel Process. Technol. 90 (2009) 889–894.

[94] Z. Sun, S. Luo, P. Qi, L.-S. Fan, Ionic diffusion through Calcite (CaCO3) layer during the reaction of CaO and CO2, Chem. Eng. Sci. 81 (2012) 164–168.

[95] J. Tanner, S. Bhattacharya, Kinetics of CO_2 and steam gasification of Victorian brown coal chars, Chem. Eng. J. 285 (2016) 331–340.

[96] Q. Wang, K. Li, Z. Guo, M. Fang, Z. Luo, K. Cen, Effects of CO_2 atmosphere on slow pyrolysis of high-ash lignite, Carbon Resources Conversion 1 (2018) 94–103.

[97] M. Lei, C. Zou, X. Xu, C. Wang, Effect of CO_2 and H_2O on the combustion characteristics and ash formation of pulverized coal in oxy-fuel conditions, Appl. Therm. Eng. 133 (2018) 308–315.

[98] Y.-L. Wang, S.-H. Zhu, M.-Q. Gao, Z.-R. Yang, L.-J. Yan, Y.-H. Bai, F. Li, A study of char gasification in H_2O and CO_2 mixtures: Role of inherent minerals in the coal, Fuel Process. Technol. 141 (2016) 9–15.

[99] S. Shi, C. Dong, W. Qin, L. Wang, W. Li, Y. Yang, Experimental and theoretical study of Fe_2O_3/coal ash oxygen carrier in CLC system, CIESC Journal 63 (2012) 4010–4018.

[100] Q. Zhou, H. Hu, Q. Liu, S. Zhu, R. Zhao, Effect of atmosphere on evolution of sulfur-containing gases during coal pyrolysis, Energy Fuel 19 (2005) 892–897.

[101] B. Galloway, B. Padak, Effect of flue gas components on the adsorption of sulfur oxides on CaO(100), Fuel 197 (2017) 541–550.

[102] E. Jerndal, T. Mattisson, A. Lyngfelt, Thermal analysis of chemical-looping combustion, Chem. Eng. Res. Des. 84 (2006) 795–806.

[103] B. Wang, R. Yan, D.H. Lee, D.T. Liang, Y. Zheng, H. Zhao, C. Zheng, Thermodynamic investigation of carbon deposition and sulfur evolution in chemical looping combustion with syngas, Energy Fuels 22 (2008) 1012–1020.

[104] C.Z. M. Lei, X. Xu, C. Wang, Effect of Fuel Gas Composition in Chemical-Looping Combustion with Ni-Based Oxygen carriers. 1. fate of sulfur, (2018).

[105] T. Zheng, M. Li, D. Mei, J. Ma, B. Wang, Z. Xu, Effect of H2S presence on chemical looping reforming (CLR) of biogas with a firebrick supported NiO oxygen carrier, Fuel Process Technol 226 (2022).

[106] I. Adánez-Rubio, A. Abad, P. Gayán, F. García-Labiano, L.F. de Diego, J. Adánez, The fate of sulphur in the Cu-based chemical looping with oxygen uncoupling (CLOU) process, Appl. Energy 113 (2014) 1855–1862.

[107] C.R. Forero, P. Gayán, F. García-Labiano, L.F. de Diego, A. Abad, J. Adánez, Effect of gas composition in chemical-looping combustion with copper-based oxygen carriers: fate of sulphur, Int. J. Greenhouse Gas Control 4 (2010) 762–770.

[108] A. Cabello, C. Dueso, F. García-Labiano, P. Gayán, A. Abad, L.F. de Diego, J. Adánez, Performance of a highly reactive impregnated Fe_2O_3/Al_2O_3 oxygen carrier with CH4 and H2S in a 500Wth CLC unit, Fuel 121 (2014) 117–125.

[109] J. Ma, D. Mei, C. Wang, X. Tian, Z. Liu, H. Zhao, Sulfur fate during in-situ gasification chemical looping combustion (iG-CLC) of coal, Chem. Eng. J. 406 (2021), 126773.

[110] C. Chung, Y. Pottimurthy, M. Xu, T.-L. Hsieh, D. Xu, Y. Zhang, Y.-Y. Chen, P. He, M. Pickarts, L.-S. Fan, A. Tong, Fate of sulfur in coal-direct chemical looping systems, Appl. Energy 208 (2017) 678–690.

[111] A.G. Basu, Behavior and Distribution of Sulfur Species in Coal-Direct Chemical Looping with Iron-Based Oxygen Carriers, in, 2020.

[112] J. Bao, Z. Li, N. Cai, Promoting the reduction reactivity of ilmenite by introducing foreign ions in chemical looping combustion, Ind. Eng. Chem. Res. 52 (2013) 6119–6128.

[113] Y. Bai, S. Zhu, K. Luo, M. Gao, L. Yan, F. Li, Coal char gasification in H_2O/CO_2: release of alkali and alkaline earth metallic species and their effects on reactivity, Appl. Therm. Eng. 112 (2017) 156–163.

[114] I. Gogolev, A.H. Soleimanisalim, D. Mei, A. Lyngfelt, Effects of temperature, operation mode, and steam concentration on alkali release in chemical looping conversion of biomass—experimental investigation in a 10 kwth pilot, Energy Fuel (2022).

[115] D. Mei, A. Lyngfelt, H. Leion, C. Linderholm, T. Mattisson, Oxygen carrier and alkali interaction in chemical looping combustion: case study using a braunite mn ore and charcoal impregnated with K_2CO_3 or Na_2CO_3, Energy Fuel (2022).

[116] X. Yao, Y. Zheng, H. Zhou, K. Xu, Q. Xu, L. Li, Effects of biomass blending, ashing temperature and potassium addition on ash sintering behaviour during co-firing of pine sawdust with a Chinese anthracite, Renew. Energy 147 (2020) 2309–2320.

[117] N.-J. Jing, Q.-H. Wang, Y.-K. Yang, L.-M. Cheng, Z.-Y. Luo, K.-F. Cen, Influence of ash composition on the sintering behavior during pressurized combustion and gasification process, J. Zheijang Univ. Sci. A 13 (2012) 230–238.

[118] B.M. Jenkins, R.R. Bakker, J.B. Wei, On the properties of washed straw, Biomass Bioenerg 10 (1996) 177–200.

[119] L. Mu, T. Li, Z. Wang, Y. Shang, H. Yin, Influence of water/acid washing pretreatment of aquatic biomass on ash transformation and slagging behavior during co-firing with bituminous coal, Energy 234 (2021).

[120] J. Zhang, X. Ma, J. Yu, X. Zhang, T. Tan, The effects of four different pretreatments on enzymatic hydrolysis of sweet sorghum bagasse, Bioresour Technol 102 (2011) 4585–4589.

[121] B. Tonn, V. Dengler, U. Thumm, H.P. Piepho, W. Claupein, Influence of leaching on the chemical composition of grassland biomass for combustion, Grass Forage Sci 66 (2011) 464–473.

[122] I. Iáñez-Rodríguez, M.Á. Martín-Lara, A. Pérez, G. Blázquez, M. Calero, Water washing for upgrading fuel properties of greenhouse crop residue from pepper, Renew Energ 145 (2020) 2121–2129.

[123] M.A. Carrillo, S.A. Staggenborg, J.A. Pineda, Washing sorghum biomass with water to improve its quality for combustion, Fuel 116 (2014) 427–431.

[124] B. Hedman, D. Boström, W. Zhu, H. Örberg, S. Xiong, Enhancing fuel qualities of cassava crop residues by washing, Fuel Process Technol 139 (2015) 127–134.

[125] B. Gudka, J.M. Jones, A.R. Lea-Langton, A. Williams, A. Saddawi, A review of the mitigation of deposition and emission problems during biomass combustion through washing pre-treatment, J Energy Inst 89 (2016) 159–171.

[126] L. Deng, T. Zhang, D. Che, Effect of water washing on fuel properties, pyrolysis and combustion characteristics, and ash fusibility of biomass, Fuel Process Technol 106 (2013) 712–720.

[127] S.S.D. Vamvuka, Degradation characteristics of straw and washed straw, Renew Energ 2433–2439 (2011).

[128] D. Vamvuka, S. Sfakiotakis, Effects of heating rate and water leaching of perennial energy crops on pyrolysis characteristics and kinetics, Renew. Energy 36 (2011) 2433–2439.

[129] D. Mazerolle, H. Rezaei, B. Bronson, L. Nguyen, F. Preto, Sieving and acid washing as a pretreatment to fast pyrolysis of a high ash hog fuel, Energ Fuel 33 (2019) 5352–5359.

[130] Y. Li, Y. Xin, X. Wang, S. Li, Fixed bed reactor pyrolysis of rape straw: effect of dilute acid pickling on the production of bio-oil and enhancement of sugars, Ind Eng Chem Res 59 (2020) 17564–17574.

[131] J.E. Aston, D.N. Thompson, T.L. Westover, Performance assessment of dilute-acid leaching to improve corn stover quality for thermochemical conversion, Fuel 186 (2016) 311–319.

[132] S. Zhang, R. Xiao, J. Liu, S. Bhattacharya, Performance of $Fe_2O_3/CaSO_4$ composite oxygen carrier on inhibition of sulfur release in calcium-based chemical looping combustion, Int. J. Greenhouse Gas Control 17 (2013) 1–12.

[133] A. Pettersson, M. Zevenhoven, B.-M. Steenari, L.-E. Åmand, Application of chemical fractionation methods for characterisation of biofuels, waste derived fuels and CFB co-combustion fly ashes, Fuel 87 (2008) 3183–3193.

[134] Y. Chiu, C. Chang, J. Lin, S. Huang, Alkaline and ultrasonic pretreatment of sludge before anaerobic digestion, Water Sci. Technol. 36 (1997).

[135] S. Fang, W. Gu, L. Chen, Z. Yu, M. Dai, Y. Lin, Y. Liao, X. Ma, Ultrasonic pretreatment effects on the co-pyrolysis of municipal solid waste and paper sludge through orthogonal test, Bioresour Technol 258 (2018) 5–11.

[136] H. Namkung, J.-H. Park, Y.-J. Lee, G.-S. Song, J.W. Choi, S.-J. Park, S. Kim, J. Liu, Y.-C. Choi, Performance evaluation of biomass pretreated by demineralization and torrefaction for ash deposition and PM emissions in the combustion experiments, Fuel 292 (2021).

[137] D. Lv, M. Xu, X. Liu, Z. Zhan, Z. Li, H. Yao, Effect of cellulose, lignin, alkali and alkaline earth metallic species on biomass pyrolysis and gasification, Fuel Process Technol 91 (2010) 903–909.

[138] A. Lyngfelt, B. Leckner, A 1000 MWth boiler for chemical-looping combustion of solid fuels – discussion of design and costs, Appl. Energy 157 (2015) 475–487.

[139] G. Sedres, Recovery of SiO_2 and Al_2O_3 from coal fly ash, Master Thesis (2016).

[140] A. Uliasz-Bochenczyk, E. Mokrzycki, The potential of FBC fly ashes to reduce CO2 emissions, Sci Rep 10 (2020) 9469.

[141] A. Phounglamcheik, R. Vila, N. Kienzl, L. Wang, A. Hedayati, M. Brostrom, K. Ramser, K. Engvall, O. Skreiberg, R. Robinson, K. Umeki, CO_2 Gasification reactivity of char from high-ash biomass, ACS Omega 6 (2021) 34115–34128.

[142] H.R. Kim, D.H. Lee, L.S. Fan, A.H. Park, Synthesis of iron-based chemical looping sorbents integrated with pH swing carbon mineral sequestration, J Nanosci Nanotechnol 9 (2009) 7422–7427.

[143] L.F. de Diego, F.G.- Labiano, P. Gayán, J. Celaya, J.M. Palacios, J. Adánez, Operation of a 10kWth chemical-looping combustor during 200h with a CuO–Al_2O_3 oxygen carrier, Fuel 86 (2007) 1036–1045.

[144] F. Garcia-Labiano, P. Gayan, J. Adanez, L.F. De Diego, C.R. Forero, Solid waste management of a chemical-looping combustion plant using Cu-based oxygen carriers, Environ Sci Technol 41 (2007) 5882–5887.

[145] C.-W. Chen, C.-Y. Chen, Preparation of monodisperse polystyrene microspheres: effect of reaction parameters on particle formation, and optical performances of its diffusive agent application, Colloid Polym. Sci. 287 (2009) 1377–1389.

[146] M. Attah, F. Hildor, D. Yilmaz, H. Leion, Vanadium recovery from steel converter slag utilised as an oxygen carrier in oxygen carrier aided combustion (OCAC), J. Clean. Prod. 293 (2021).

[147] L.F. de Diego, F.G.- Labiano, P. Gayán, J. Celaya, J.M. Palacios, J. Adánez, Operation of a 10 kWth chemical-looping combustor during 200 h with a CuO–Al_2O_3 oxygen carrier, Fuel 86 (2007) 1036–1045.

[148] W. Qiye, G. Weiping, J. Yun, Preparation of monodis- perse cross-linked PS nano-microspheres by emulsifier-free emulsion polymerization, China Plastics Industry 28 (2000) 21–23.

[149] M. Sadakane, R. Kato, T. Murayama, W. Ueda, Preparation and formation mechanism of three-dimensionally ordered macroporous (3DOM) MgO, MgSO4, CaCO3, and SrCO3, and photonic stop band properties of 3DOM CaCO3, J. Solid State Chem. 184 (2011) 2299–2305.

[150] K. Zhao, H.E. Fang, H. z,, Support info of Biomass pyrolysis/gasification using three dimensional ordered macroporous (3DOM) Fe2O3 as an oxygen carrier, J Fuel Chem Technol 041 (2013) 277–284.

[151] R.Y. Abrokwah, V.G. Deshmane, D. Kuila, Comparative performance of M-MCM-41 (M: Cu Co, Ni, Pd, Zn and Sn) catalysts for steam reforming of methanol, J. Mol. Catal. A Chem. 425 (2016) 10–20.

[152] D. Li, L. Zeng, X. Li, X. Wang, H. Ma, S. Assabumrungrat, J. Gong, Ceria-promoted Ni/SBA-15 catalysts for ethanol steam reforming with enhanced activity and resistance to deactivation, Appl Catal B 176–177 (2015) 532–541.

[153] B. Jiang, B. Dou, K. Wang, Y. Song, H. Chen, C. Zhang, Y. Xu, M. Li, Hydrogen production from chemical looping steam reforming of glycerol by Ni based Al-MCM-41 oxygen carriers in a fixed-bed reactor, Fuel 183 (2016) 170–176.

[154] K. Wang, B. Dou, B. Jiang, Y. Song, C. Zhang, Q. Zhang, H. Chen, Y. Xu, Renewable hydrogen production from chemical looping steam reforming of ethanol using xCeNi/SBA-15 oxygen carriers in a fixed-bed reactor, Int. J. Hydrogen Energy 41 (2016) 12899–12909.

[155] P. Sirinwaranon, D. Atong, V. Sricharoenchaikul, Gasification of torrefied cassava rhizome with Ni/MCM-41 catalyst derived from illite waste, Energy Rep. 6 (2020) 537–547.

[156] S. Daneshmand-Jahromi, M. Meshksar, A. Hafizi, M.R. Rahimpour, Synthesis, characterization and application of Ni-based oxygen carrier supported on novel yttrium-incorporated SBA-16 for efficient hydrogen production via chemical looping steam methane reforming, J. Taiwan Inst. Chem. Eng. 89 (2018) 129–139.

[157] X. Cao, J. Zhao, F. Long, X. Zhang, J. Xu, J. Jiang, Al-modified Pd@mSiO_2 core-shell catalysts for the selective hydrodeoxygenation of fatty acid esters: Influence of catalyst structure and Al atoms incorporation, Appl Catal B 305 (2022).

[158] Z. Li, M. Li, J. Ashok, S. Kawi, NiCo@NiCo phyllosilicate@CeO_2 hollow core shell catalysts for steam reforming of toluene as biomass tar model compound, Energ. Conver. Manage. 180 (2019) 822–830.

[159] R.-X. Yang, L.-R. Xu, S.-L. Wu, K.-H. Chuang, M.-Y. Wey, Ni/SiO_2 core–shell catalysts for catalytic hydrogen production from waste plastics-derived syngas, Int. J. Hydrogen Energy 42 (2017) 11239–11251.

[160] S. Das, J. Ashok, Z. Bian, N. Dewangan, M.H. Wai, Y. Du, A. Borgna, K. Hidajat, S. Kawi, Silica-Ceria sandwiched Ni core–shell catalyst for low temperature dry reforming of biogas: Coke resistance and mechanistic insights, Appl Catal B 230 (2018) 220–236.

[161] J. Hu, C. Li, Q. Zhang, Q. Guo, S. Zhao, W. Wang, D.-J. Lee, Y. Yang, Using chemical looping gasification with Fe2O3/Al2O3 oxygen carrier to produce syngas (H2+CO) from rice straw, Int. J. Hydrogen Energy 44 (2019) 3382–3386.

[162] X. Huang, Z. Hu, Z. Miao, E. Jiang, X. Ma, Chemical looping gasification of rice husk to produce hydrogen-rich syngas under different oxygen carrier preparation methods, Int. J. Hydrogen Energy 45 (2020) 26865–26876.

[163] K. Wang, Q. Yu, Q. Qin, L. Hou, W. Duan, Thermodynamic analysis of syngas generation from biomass using chemical looping gasification method, Int. J. Hydrogen Energy 41 (2016) 10346–10353.

[164] E. Bazhenova, K. Honkala, Screening the bulk properties and reducibility of Fe-doped Mn_2O_3 from first principles calculations, Catal. Today 285 (2017) 104–113.

[165] P.G. Loutzenhiser, M.E. Gálvez, I. Hischier, A. Stamatiou, A. Frei, A. Steinfeld, CO_2 splitting via two-step solar thermochemical cycles with Zn/ZnO and FeO/Fe_3O_4 redox reactions II: kinetic analysis, Energy Fuel 23 (2009) 2832–2839.

[166] N. Alarcón, X. García, M.A. Centeno, P. Ruiz, A. Gordon, New effects during steam gasification of naphthalene: the synergy between CaO and MgO during the catalytic reaction, Appl. Catal. A 267 (2004) 251–265.

[167] J. Delgado, M.P. Aznar, J. Corella, Biomass gasification with steam in fluidized bed: effectiveness of CaO, MgO, and CaO−MgO for hot raw gas cleaning, Ind. Eng. Chem. Res. 36 (1997) 1535–1543.

[168] G. Liu, Y. Liao, Y. Wu, X. Ma, Synthesis gas production from microalgae gasification in the presence of Fe_2O_3 oxygen carrier and CaO additive, Appl. Energy 212 (2018) 955–965.

[169] Z. Chen, Y. Liao, G. Liu, F. Mo, X. Ma, Application of Mn–Fe composite oxides loaded on alumina as oxygen carrier for chemical looping gasification, Waste Biomass Valoriz. 11 (2019) 6395–6409.
[170] B. Wang, H. Zhao, Y. Zheng, Z. Liu, C. Zheng, Chemical looping combustion of petroleum coke with $CuFe_2O_4$ as oxygen carrier, Chem. Eng. Technol. 36 (2013) 1488–1495.
[171] S. Liu, F. He, Z. Huang, A. Zheng, Y. Feng, Y. Shen, H. Li, H. Wu, P. Glarborg, Screening of $NiFe_2O_4$ Nanoparticles as Oxygen Carrier in Chemical Looping Hydrogen Production, Energy Fuel 30 (2016) 4251–4262.
[172] Y.-L. Kuo, W.-M. Hsu, P.-C. Chiu, Y.-H. Tseng, Y. Ku, Assessment of redox behavior of nickel ferrite as oxygen carriers for chemical looping process, Ceram. Int. 39 (2013) 5459–5465.
[173] D. Zeng, Y. Qiu, S. Peng, C. Chen, J. Zeng, S. Zhang, R. Xiao, Enhanced hydrogen production performance through controllable redox exsolution within CoFeAlOx spinel oxygen carrier materials, J. Mater. Chem. A 6 (2018) 11306–11316.
[174] Q. Shen, Y. Zheng, C. Luo, C. Zheng, Characteristics of SrCo1-xFexO3-δPerovskite powders with improved O_2/CO_2 production performance for oxyfuel combustion, Bull. Kor. Chem. Soc. 35 (2014) 1613–1618.
[175] Q. Shen, Y. Zheng, C. Luo, C. Zheng, Development and characterization of $Ba_{1-x}Sr_xCo_{0.8}Fe_{0.2}O_{3-\delta}$ perovskite for oxygen production in oxyfuel combustion system, Chem Eng J 255 (2014) 462–470.
[176] L. Jiang, S. Hu, Y. Wang, S. Su, L. Sun, B. Xu, L. He, J. Xiang, Catalytic effects of inherent alkali and alkaline earth metallic species on steam gasification of biomass, Int. J. Hydrogen Energy 40 (2015) 15460–15469.
[177] H. Ding, Y. Xu, C. Luo, Y. Zheng, Q. Shen, Z. Liu, L. Zhang, Synthesis and characteristics of BaSrCoFe-based perovskite as a functional material for chemical looping gasification of coal, Int. J. Hydrogen Energy 41 (2016) 22846–22855.